AD_____

Award Number: W81XWH-07-1-0153

TITLE: Examination of the Role of DNA Methylation Changes in Prostate Cancer using the Transgenic Adenocarcinoma of Mouse Prostate (TRAMP) Model

PRINCIPAL INVESTIGATOR: Shannon R. Morey

CONTRACTING ORGANIZATION: Roswell Park Cancer Institute
Buffalo, NY 14263

REPORT DATE: March 2008

TYPE OF REPORT: Annual Summary

PREPARED FOR: U.S. Army Medical Research and Materiel Command
Fort Detrick, Maryland 21702-5012

REPORT DOCUMENTATION PAGE

Form Approved
OMB No. 0704-0188

1. REPORT DATE *(DD-MM-YYYY)*	**2. REPORT TYPE**	**3. DATES COVERED** *(From - To)*
01-03-2008	Annual Summary	1 MAR 2007 - 28 FEB 2008

4. TITLE AND SUBTITLE

Examination of the Role of DNA Methylation Changes in Prostate Cancer using the Transgenic Adenocarcinoma of Mouse Prostate (TRAMP) Model

5a. CONTRACT NUMBER

5b. GRANT NUMBER
W81XWH-07-1-0153

5c. PROGRAM ELEMENT NUMBER

6. AUTHOR(S)
Shannon R. Morey

E-Mail: Shannon.MoreyKinney@RoswellPark.org

5d. PROJECT NUMBER

5e. TASK NUMBER

5f. WORK UNIT NUMBER

7. PERFORMING ORGANIZATION NAME(S) AND ADDRESS(ES)

Roswell Park Cancer Institute
Buffalo, NY 14263

8. PERFORMING ORGANIZATION REPORT NUMBER

9. SPONSORING / MONITORING AGENCY NAME(S) AND ADDRESS(ES)
U.S. Army Medical Research and Materiel Command
Fort Detrick, Maryland 21702-5012

10. SPONSOR/MONITOR'S ACRONYM(S)

11. SPONSOR/MONITOR'S REPORT NUMBER(S)

12. DISTRIBUTION / AVAILABILITY STATEMENT
Approved for Public Release; Distribution Unlimited

13. SUPPLEMENTARY NOTES

14. ABSTRACT
The TRansgenic Adenocarcinoma of Mouse Prostate (TRAMP) model provides an excellent system to study disruption of the DNA methylation process in prostate cancer. To date, several key conclusions can be made from this research. First, analysis of methylation patterns in TRAMP revealed a small number of hypermethylation events in early stage lesions, with a great increase in late stage tumors. Furthermore, late stage tumors, androgen independent tumors and metastases each display numerous and tumor type specific hypermethylation events. Secondly, a large proportion of these hypermethylated genes, including p19/ARF and p16INK4a, display downstream hypermethylation correlating with robust overexpression. In addition, p16 and p19 overexpression, but not downstream hypermethylation, occurs in early stage prostatic lesions in TRAMP, suggesting that overexpression may be the initiating event and pharmacological reversal of downstream hypermethylation in TRAMP cell lines led to decreased expression of p19 and p16, indicating that downstream hypermethylation contributes to the maintenance of increased gene expression. Overall these data indicate that locus specific hypermethylation is selected for upon tumor progression and treatment with hypomethylating agents may inactivate oncogenes whose expression is maintained by downstream hypermethylation.

15. SUBJECT TERMS
Prostate cancer, DNA methylation, Transgenic Adenocarcinoma of Mouse Prostate (TRAMP)

16. SECURITY CLASSIFICATION OF:			**17. LIMITATION OF ABSTRACT**	**18. NUMBER OF PAGES**	**19a. NAME OF RESPONSIBLE PERSON**
a. REPORT	**b. ABSTRACT**	**c. THIS PAGE**			USAMRMC
U	U	U	UU	63	**19b. TELEPHONE NUMBER** *(include area code)*

Table of Contents

Introduction:

DNA hypermethylation of tumor suppressor gene promoters, in conjunction with hypomethylation of repetitive elements and increased expression of DNA methyltransferases (DNMTs), occurs in human prostate cancer. An understanding of how DNA methylation becomes deregulated in prostate cancer and how to reverse or prevent this process is important for developing anticancer therapies. It has also been shown that pharmacological inhibition of DNMTs can have anticancer effects, supporting the concept that hypomethylation and thus reexpression of tumor suppressor genes may have therapeutic significance in the treatment of cancer. The TRansgenic Adenocarcinoma of Mouse Prostate (TRAMP) SV40 transgenic autochthonous model, along with clonal cell lines derived from TRAMP primary tumors, provides an excellent system to study disruption of the DNA methylation process in prostate cancer and to determine whether inhibition of DNMTs abrogates prostate tumorigenesis. Our preliminary data suggest that DNA methylation is deregulated in the TRAMP model, which is characterized by altered methylation patterning of CpG islands and significantly increased DNMT activity and expression. Based on these findings, we hypothesize that aberrant DNA methylation contributes to TRAMP tumorigenesis, and that disruption of DNMTs will inhibit prostate oncogenesis in TRAMP. The information gained from this study will permit a better understanding of the role of aberrant DNA methylation in prostate cancer.

Specific Aims:

1. Identify and characterize the biological significance of genes that have altered DNA methylation status in TRAMP.
2. Determine whether genetic disruption of DNMT1 inhibits prostate tumorigenesis in TRAMP.

Body:

Examination of the Role of DNA Methylation Changes in Prostate Cancer using the Transgenic Adenocarcinoma of Mouse Prostate (TRAMP) Model

Task 1. Identify and characterize the biological significance of genes that have altered DNA methylation status in TRAMP:

To complete this task I analyzed several types of TRAMP samples including Prostatic Intraepithelial Neoplasia (PIN), Well Differentiated disease (WD), Early and Late Poorly Differentiated disease (EPD and LPD), Androgen Independent Primary (AIP) tumors and metastases from liver and lung (MET) (1-3). I then performed RLGS spot cloning to identify several loci that were commonly methylated in these different types of TRAMP tumors (Appended publications 1 and 2, (1, 3). While several of the identified genes were hypermethylated in the promoter region, a very high percentage of these genes showed hypermethylation of downstream regions rather than in the promoter of the gene (Table 1, 2, (1, 3)).

I next performed qRT-PCR analysis to determine the expression of several of the commonly hypermethylated genes from the previous task. I examined those that displayed hypermethylation by RLGS analysis of either the promoter region or downstream regions. From these experiments I did not identify any genes that showed promoter region hypermethylation with correlating decreased expression. Therefore, the only gene fitting these criteria that I have identified in TRAMP is the IRX3 gene (Figure 1, (2)). However, I did identify six genes that display downstream hypermethylation correlating with increased expression, which we reported in two publications included in the appendix (1-3). These genes include p19, p16, Cacna1a, Gsc, Nrxn2, and the unknown gene BC058385 (1-3). Perhaps the most interesting of these are p19 and p16 which are both encoded in the CDKN2A locus, since this locus was hypermethylated in almost all PD, AIP and Met tumors. I find that when these genes are overexpressd in LPD, AIP, or MET tumors they are hypermethylated in the third exon (Figure 2a-b, (1, 2)). I also find that these genes are overexpressed in PIN and WD samples that are not hypermethylated (Figure 2c-d, Table 1, (3)). These results suggest that the overexpression occurs prior to and may lead to the downstream hypermethylation. I also examined the expression of the six genes listed above in the C2D and C2N cell lines. The only genes that were expressed in these cell lines were *p19* and *p16*. Furthermore when the cell lines were treated with a hypomethylating agent (5-aza-2'-deoxycytidine, DAC) the expression of both *p19* and *p16* was decreased (Figure 3a and data not shown). I also found that the CDKN2A locus is hypermethylated in TRAMP cell lines and this methylation is decreased when treated with DAC (Figure 3b).

I then completed further methylation analyses on the downstream hyper-methylated region identified by RLGS as well as the promoter region for p19, p16, Cacna1a, Gsc, Nrxn2, and the unknown gene BC058385 (Figure 4 and appended publications (1, 3)). This was completed either through traditional bisulfite sequencing or Mass Array Quantitative Methylation Analysis (MAQMA) which is also based on the bisulfite conversion of DNA. However, no further methylation analysis was completed on genes identified by RLGS to have promoter hypermethylation since for none of these

genes was there any correlation with decreased expression. Bisulfite sequencing confirmed the RLGS results that the downstream regions were hypermethylated and that the promoters were unmethylated for each gene (Figure 4 and appended publications (1, 3)).

I have not completed the later proposed experiments in this task (D and E) due to the unexpected results described above. However, I am currently performing methyl-DIP chip array analyses on TRAMP tumors versus normal prostate to identify novel genes that display promoter hypermethylation correlating with decreased expression in TRAMP.I proposed this technique in the alternative approaches in the situation that RLGS analysis was not sufficient to identify such genes. The idea is that this more global approach where there are no limitations on gene identification will lead us to genes that fit the specific criteria. In addition to methyl-DIP chip analyses I am currently examining several candidate tumor suppressor genes that are commonly hypermethylated in the promoter region associated with decreased expression, in human prostate cancer. These genes are Aldh1a2, Zfp185, Mgmt, Pdlim4, Rarres1, and Vegfr1. I hope to find that some of these genes are also hypermethylated in TRAMP to confirm that this phenomenon occurs in this model and as a set of genes that we can analyze in the Dnmt1 hypomorphic TRAMP mice to determine if DNA methylation changes that occur during TRAMP tumorigenesis are inhibited.

Task 2. Determine whether genetic disruption of DNA methyltransferase 1 (DNMT1) inhibits prostate tumorigenesis in TRAMP:

I did obtain C57Bl/6 mice carrying either the N or R Dnmt1 hypomorphic allele From Dr. Peter Laird and have produced sufficient mice in this breeding colony to complete the proposed experiments. The experimental design to characterize phenotype of DNMT1 hypomorphic mouse prostates and epigenetic parameters was to obtain a samples set of at least three mice for each possible genotype (WT, N/+, R/+, N/R) at either 15 or 24 weeks of age to analyze histologically for prostate development, for DNA hypomethylation at a global level, and for Dnmt protein expression. These experiments are nearly complete. However, the Dnmt1 hypomorphic alleles (N and R) are not inherited in a mendelian ratio (should be 1:1:1:1 for each genotype, WT, N/+, R/+, N/R), which was not previously reported. Mice having both the N and R alleles have the least amount of DNmt1 expression and therefore may show an altered phenotype compared to N/+ or R/+ which have only slightly less than normal Dnmt1 expression. Unfortunately N/R mice are found at much lower than expected (one fifth of expected) making these experiments take much longer than previously estimated (Table 3). I also analyzed animal weight, urogenital (UG) weight, and prostate weight in these animals and found that there is a significant decrease in all three parameters in N/R mice compared to WT mice at 15 weeks and in animal and UG weight at 24 weeks of age (Figure 5). The only other significant change observed was a decrease in UG weight in N/+ mice at 15 weeks. This may be explained by the observation that, overall there seems to be more difference at 15 weeks of age versus 24 weeks and that the N/+ mice have been shown to have less Dnmt1 expression than R/+ mice.

Hematoxylin and eosin staining of prostate and liver in the Dnmt1 hypomorphic mice shows a normal morhology in WT, N/+, R/+ at 15 and 24 weeks of age and in N/R

mice at 15 weeks of age. I do not have samples for histology for N/R mice at 24 weeks of age due to the decreased Mendelian inheritance, but will obtain them shortly. Once the rest of N/R samples are collected I will perform immunohistochemical analysis for the proliferative marker Ki67 and other cell specific markers within the prostate to determine if the Dnmt1 hypomorphic prostates display a normal phenotype.

In order to confirm that the genotype was correlated with the expected phenotype of DNA hypomethylation, I next measured global methylation (%5mdC/dG) in both prostate and liver tissues from the Dnmt1 hypomorphic mice at either 15 or 24 weeks of age. As expected, global hypomethylation is observed in N/R mice with slight hypomethylation in N/+ mice, with more hypomethylation at the earlier time point (Figure 7). I am currently completing western blot analyses of Dnmt1, Dnmt3a, and Dnmt3b proteins in samples from the four genotypes at either 15 or 24 weeks of age.

The second part of this task is to produce 50:50 C57Bl/6 x FVB DNMT1 hypomorphic TRAMP mice. There are two breeding strategies for this. The first is a single cross of C57Bl/6 mice carrying either the N or R Dnmt1 hypomorphic allele to FVB TRAMP mice to produce 50:50 C57Bl/6 x FVB TRAMP mice carrying one DNMT1 hypomorphic allele. The second is to transfer the Dnmt1 hypomorphic alleles from the C57Bl/6 background to the TRAMP FVB background. These mice can then be backcrossed to C57Bl/6 mice carrying one Dnmt1 hypomorphic allele to produce 50:50 C57Bl/6 x FVB TRAMP mice carrying both DNMT1 hypomorphic alleles (N/R).

I have collected tissue samples from several Dnmt1 hypomorphic TRAMP mice from the first breeding strategy at either 15 or 24 weeks of age. These mice can have one of three possible genotypes (WT, N/+, or R/+). The data collected at necropsy (animal weight, urogenital weight, prostate weight) show a statistically significant decrease in all three parameters in N/+ mice compared to WT mice at the 15 week timepoint, which is not seen at 24 weeks of age (Figure 8).

The time it would take to produce the mice in the original second breeding strategy is in the order of years. Therefore, the number of backcrosses has been decreased from 7 to 4. The f4 mice are 93.75% FVB and offspring of a cross to C57 would be 46.9% FVB:53.1% C57. Because these mice are not purely 50:50 I will only use non-hypomorphic littermates as controls and will not collect any more of samples from the first breeding strategy. I am currently collecting samples at either 15 or 24 weeks of age from the 46.9% FVB:53.1% C57 mice which carry the TRAMP transgene and are of four possible Dnmt1 hypomorphic phenotypes (WT, N/+, R/+, N/R). Based on the finding that both Dnmt1 alleles are not inherited in mendelian fashion I will increase the number of breeding cages to obtain enough mice for this study. Once these samples are available I will begin characterizing the epigenetic parameters proposed for this task.

Key Research Accomplishments:

Key Scientific Findings:

- Restriction Landmark Genomic Scanning (RLGS) analysis of methylation patterns in TRAMP revealed a small number of hypermethylation events in PIN and WD lesions, with a great increase in EPD and LPD tumors.
- LPD, AIP and MET tumor phenotypes each display numerous hypermethylation events, with the most homogeneous hypermethylation pattern in AIP tumors and the most heterogeneous hypermethylation pattern in metastases.
- There are several loci that displayed a tumor phenotype specific methylation status, suggesting that selection may play a role in the development of these patterns.
- Hypermethylated genes revealed by RLGS showed hypermethylation of downstream exons correlating with mRNA overexpression.
- BC058385, Goosecoid (GSC), p19/ARF, p16INK4a, NRXN2 and Cacna1a display downstream hypermethylation correlating with robust mRNA overexpression.
- Overexpression of *p16* and *p19,* but not downstream hypermethylation, occurs in early stage prostatic lesions in TRAMP, suggesting that gene overexpression is the initiating event.
- Pharmacological reversal of downstream gene hypermethylation in TRAMP cell lines led to decreased expression of *p19* and *p16*, suggesting that downstream hypermethylation contributes to the maintenance of increased gene expression.
- N/R Dnmt1 Hypomorphic genotype is not inherited in Mendelian fashion
- N/R mice and less significantly N/+ mice are smaller in size and have decreased UG weight and prostate weight than WT mice
- N/R mice have significant hypomethylation in prostate and liver tissues compared to WT mice
- The differences between Dnmt1 hypomorphs and WT mice are more distinct at 15 weeks than 24 weeks of age

Resources:

- Gene list of commonly hypermethylated loci in TRAMP from RLGS analysis
- Dnmt1 hypomorphic mouse colony (C57Bl/6)
- Dnmt1 hypomorphic TRAMP mouse colony (FVB)

Reportable Outcomes:

Manuscripts

Morey Kinney, Shannon R., Dominic J. Smiraglia, Smitha R. James, Michael T. Moser, Barbara A. Foster, and Adam R. Karpf. Stage-specific alterations of Dnmt expression, DNA hypermethylation, and DNA hypomethylation during prostate cancer progression in the TRAMP model. Molecular Cancer Res. *In press*. 2008

Marta Camoriano ***, Shannon R. Morey Kinney***, Michael T. Moser, Barbara A. Foster, James L. Mohler, Donald L. Trump, Adam R. Karpf, and Dominic J. Smiraglia. Cancer Research. *In press.* 2008.
*Equal contribution

Presentations

Shannon R. Morey. Cancer Epigenetics as Seen Through the Eyes of a Mouse. Invited lecture 2007 Science Decade Lecture Series, Roswell Park Cancer Institute, March 6, 2007

Shannon R. Morey, Dominic J. Smiraglia, Barbara A. Foster, and Adam R. Karpf. Alterations in DNA Methylation During TRAMP Tumor Progression. Oral presentation at the Annual Pharmacology Sciences Day, University at Buffalo, May 14, 2007.

Shannon R. Morey, Dominic J. Smiraglia, Michael T. Moser, Barbara A. Foster, and Adam R. Karpf. DNA Methylation Pathway Alterations in a Mouse Model of Prostate Cancer. Poster presentation at the AACR Edward A. Smuckler Memorial Pathobiology of Cancer Workshop, Snowmass, CO, July 18, 2007.

Shannon R. Morey Kinney, Dominic J. Smiraglia, Michael T. Moser, Barbara A. Foster, and Adam R. Karpf. Comparison of Altered DNA Methylation During Prostate Cancer Progression Using the TRAMP Model. Poster presentation at the Pharmacology and Therapeutics Departmental Retreat. Holiday Valley Resort and Conference Center, Ellicottville, NY, November 8, 2007.

Shannon R. Morey Kinney, Dominic J. Smiraglia, Michael T. Moser, Barbara A. Foster, and Adam R. Karpf. Comparison of Altered DNA Methylation During Prostate Cancer Progression Using the TRAMP Model. Poster presentation at the 14th Annual Thanksgiving Poster Forum. Roswell Park Cancer Institute, Buffalo, NY, November 16, 2007.

Shannon R. Morey Kinney, Marta Camoriano, Michael T. Moser, Barbara A. Foster, Dominic J. Smiraglia, and Adam R. Karpf. Restriction Landmark Genomic Scanning Reveals Phenotype Specific Epigenomic Patterns in a Mouse Model of Prostate Cancer. Poster presentation at the Keystone Cancer Genomics and Epigenomics Symposium, Taos, NM, February 21, 2008.

Funding

SUM-07-14 Mark Diamond Research Fund Award, University at Buffalo
"Epigenetic Deregulation in a Mouse Model of Prostate Cancer"

Conclusion:

While I was not able to identify any genes in addition to Irx3 that are hypermethylated in the promoter correlating with decreased expression in TRAMP, I did identify several genes that have increased expression that correlates with downstream hypermethylation. This phenomenon has been shown to occur in plants, but has not been well studied in mammals or cancer models. These data have been accepted for publication through peer review, indicating the importance of these unexpected findings.

These results indicate that altered DNA methylation may play an important role in increased gene expression in addition to the well studied decreased gene expression. The overexpression of these genes may promote tumorigenesis and studies examining the oncogenic activity of these overexpressed genes in prostate cancer may lead us to identify novel therapeutic targets. Furthermore, these data suggest that treatment with hypomethylating agents may have dual activity of activating hypermethylated tumor suppressor genes as well as inactivating oncogenes whose expression is maintained by downstream hypermethylation. Future studies will be required to rigorously test this hypothesis.

The previously unreported knowledge that the N/R Dnmt1 hypomorphic alleles are not inherited in Mendelian fashion as well as the knowledge that these mice seem to be runted to a certain extent will be very useful in completing the second task of this study. It is also important to report a complete characterization of this model.

References:

1. Camoriano, M., Shannon R. Morey Kinney, Michael T. Moser, Barbara A. Foster, James L. Mohler, Donald L. Trump, Adam R. Karpf, and Dominic J. Smiraglia. (2008). Phenotype-specific CpG Island Methylation Events in a Murine Model of Prostate Cancer. Cancer Research, *In Press*.
2. Morey, S. R., Smiraglia, D. J., James, S. R., Yu, J., Moser, M. T., Foster, B. A., and Karpf, A. R. (2006). DNA methylation pathway alterations in an autochthonous murine model of prostate cancer. Cancer Res, *66:* 11659-11667.
3. Morey Kinney, S. R., Dominic J. Smiraglia, Smitha R. James, Michael T. Moser, Barbara A. Foster, and Adam R. Karpf. (2008). Stage-specific alterations of Dnmt expression, DNA hypermethylation, and DNA hypomethylation during prostate cancer progression in the TRAMP model. Molecular Cancer Research, *In Press*.

Appendix

Table 1. RLGS spot loss in TRAMP samples

	Number of times hypermethylated (%)						
Spot ID	PIN n = 5	WD n = 6	EPD n = 7	LPD n = 14	Gene Name	Gene Context of Hypermethylation	Hypermethylation in CpG Island
3D22	0 (0)	0 (0)	7 (100)	14 (100)	*Cdkn2a*	3' end	no
4C13	0 (0)	0 (0)	5 (71)	13 (93)	*AK039621*	5'end	yes
3D67	0 (0)	0 (0)	6 (86)	12 (86)	*Oprd1*	3' end	yes
3C21	0 (0)	0 (0)	6 (86)	10 (71)	*Nrxn2*	5' end	yes
4C31	0 (0)	0 (0)	7 (100)	10 (71)	*Adcy5*	Body	no
3E30	0 (0)	0 (0)	7 (100)	10 (71)	*Gsc*	3' end	yes
2G63	0 (0)	0 (0)	6 (86)	10 (71)	*BC051947*	Body	yes
2C28	1 (20)	4 (67)	3 (43)	9 (64)	*AK004006*	5'end	yes
5F09	0 (0)	0 (0)	3 (43)	9 (64)	*Cacna1a*	3’ end	no
5B30	0 (0)	0 (0)	5 (71)	8 (57)	*ARHGEF17*	5'end	yes
2B37	0 (0)	0 (0)	1 (14)	7 (50)	*Ptprs*	Body	yes
4C01	0 (0)	0 (0)	2 (29)	7 (50)	*AK044818*	5'end	yes
6C17	0 (0)	0 (0)	1 (14)	6 (43)	*Foxd3*	5' end	yes
4D27	0 (0)	0 (0)	0 (0)	6 (43)	*Hoxa2*	5' end	yes
4C11	0 (0)	0 (0)	3 (43)	6 (43)	*4932416N17Rik*	Body	no
5D52	0 (0)	0 (0)	0 (0)	5 (36)	*Zar1*	5' end	yes
2D39	0 (0)	0 (0)	0 (0)	5 (36)	*CG869761*	5'end	yes
4C17	0 (0)	0 (0)	3 (43)	5 (36)	*Lhfpl4*	5'end	yes
2D21	0 (0)	0 (0)	1 (14)	5 (36)	*BC025575*	3'end	yes
4G73	0 (0)	0 (0)	2 (29)	5 (36)	*Irx3*	5'end	yes
4C38	0 (0)	0 (0)	1 (14)	4 (29)	*Lhfpl4*	5'end	yes
3D36	0 (0)	0 (0)	1 (14)	4 (29)	*Lmln*	5' end	yes

Table 1 RLGS spots of interest.

#	Spot	PRIM n=30	MET n=30	AIP n=30	Total n=90	Class	[d]P-value	[e]CGI	Context	[h]Gene Homology
1	3C21	**20**	1	**27**	48	[a]Prim or AIP	**1.0E-12**	Y	Body	**Nrxn2**
2	3E30	**24**	5	**29**	58	Prim or AIP	**2.3E-11**	N	3'end	**Gsc**
3	5F09	**19**	2	**21**	42	Prim or AIP	**2.5E-08**	N	Body	**Cacna1a**
4	2G63	**22**	8	**29**	59	Prim or AIP	**7.1E-08**	Y	Body	**BC058385**
5	2B37	**14**	1	**14**	29	Prim or AIP	**1.0E-05**	[f]--	--	**--**
6	5B30	**20**	6	**22**	48	Prim or AIP	**1.2E-05**	Y	Body	**AK139829**
7	4D27	**16**	6	**19**	41	Prim or AIP	**7.0E-04**	Y	[g]5'end	**Hoxa2**
8	3E16	**8**	0	**8**	16	Prim or AIP	**9.1E-04**	--	--	**--**
9	4C01	**18**	9	**20**	47	Prim or AIP	**3.0E-03**	Y	5'end	**AK044818**
10	3D01	**7**	0	**7**	14	Prim or AIP	**3.0E-03**	--	--	**--**
11	2G10	**8**	0	**6**	14	Prim or AIP	**3.8E-03**	--	--	**--**
12	2C17	**7**	0	**5**	12	Prim or AIP	**7.0E-03**	--	--	**--**
13	4C17	**13**	8	**20**	41	Prim or AIP	**1.4E-02**	Y	5' end	**Lhfpl4**
14	4D69	0	0	**9**	9	[b]AIP specificity	**2.0E-05**	Y	5'end	**Nfyb**
15	4E04	2	4	**15**	21	AIP specificity	**5.0E-05**	Y	5'end	**Tpm2**
16	4D54	0	5	**14**	19	AIP specificity	**6.0E-05**	Y	5'end	**Pawr**
17	4E16	0	1	**9**	10	AIP specificity	**1.0E-04**	Y	5'end	**Tpm2**
18	3C39	0	0	**7**	7	AIP specificity	**2.0E-04**	Y	5'end	**Mid1ip1**
19	3G88	5	2	**13**	20	AIP specificity	**1.0E-03**	Y	5'end	**Il6st**
20	3D22	29	23	30	**82**	[c]Frequency		N	3'end	**Cdkn2a**
21	4C11	21	25	28	**74**	Frequency		N	Body	**4932416N17Rik**
22	4E25	23	25	26	**74**	Frequency		--	--	**--**
23	4C38	19	15	28	**62**	Frequency		Y	5' end	**Lhfpl4**
24	4C31	23	11	25	**59**	Frequency		N	Body	**Adcy5**
25	4C13	23	9	26	**58**	Frequency		Y	5'end	**AK039621**
26	3D67	18	17	21	**56**	Frequency		Y	3'end	**Oprd1**
27	2C28	16	14	22	**52**	Frequency		Y	5'end	**AK004006**
28	2E04	19	9	13	**41**	Frequency		--	--	**--**
29	2D21	13	8	15	**36**	Frequency		Y	3'end	**BC025575**
30	3E56	9	11	15	**35**	Frequency		Y	5' end	**Zfp787**
31	3E07	7	12	16	**35**	Frequency		Y	5'end	**U2af1-rs1**
32	6D10	6	12	15	**33**	Frequency		N	Intergenic	**Intergenic**

[a]Spots lost significantly in primary tumors plus androgen-independent primary tumors (n=60), but not metastatic tumors (n=30); [b]Spots lost significantly in androgen-independent primary tumors (n=30), but not in primary plus metastatic tumors (n=60); [c]Spots lost in greater than 30 samples from all tumor types (n=90); [d]Fischer's Exact test (two-tailed) for class membership; [e]Is the RLGS spot NotI site within 200bp of a CpG island; [f]RLGS spot is unidentified; [g]Within 5kb of transcriptional start site and/or including exon 1; [h]Annotated gene, mRNA, or spliced EST within 5 kb of the CpG island or NotI site.

Figure 1. Promoter methylation of Iroquiox Homeobox Gene 3 (IRX3) is associated with decreased expression in TRAMP tumors. A) Upper: Diagram of IRX3 gene. Right arrow, transcriptional start site; open rectangles, exons; lines, introns; vertical arrow, position of the NotI site identified by RLGS; black bar, CpG island; horizontal line with circles, regions analyzed by sodium bisulfite sequencing.Lower: Methylation analysis of NotI site identified to be hypermethylated by RLGS analysis and region upstream of transcriptional start site by bisulfite sequencing. Each circle indicates a CpG, with each row of circles indicating a sequenced clone. N – Normal prostate, LPD - Late Poorly Differentiated. Filled circles indicate methylated CpGs and unfilled circles indicate unmethylated CpGs. B) qRT-PCR expression analysis of IRX3 in TRAMP tumors compared to normal prostate. Filled bars are those that were shown to be hypermethylated by RLGS analysis.

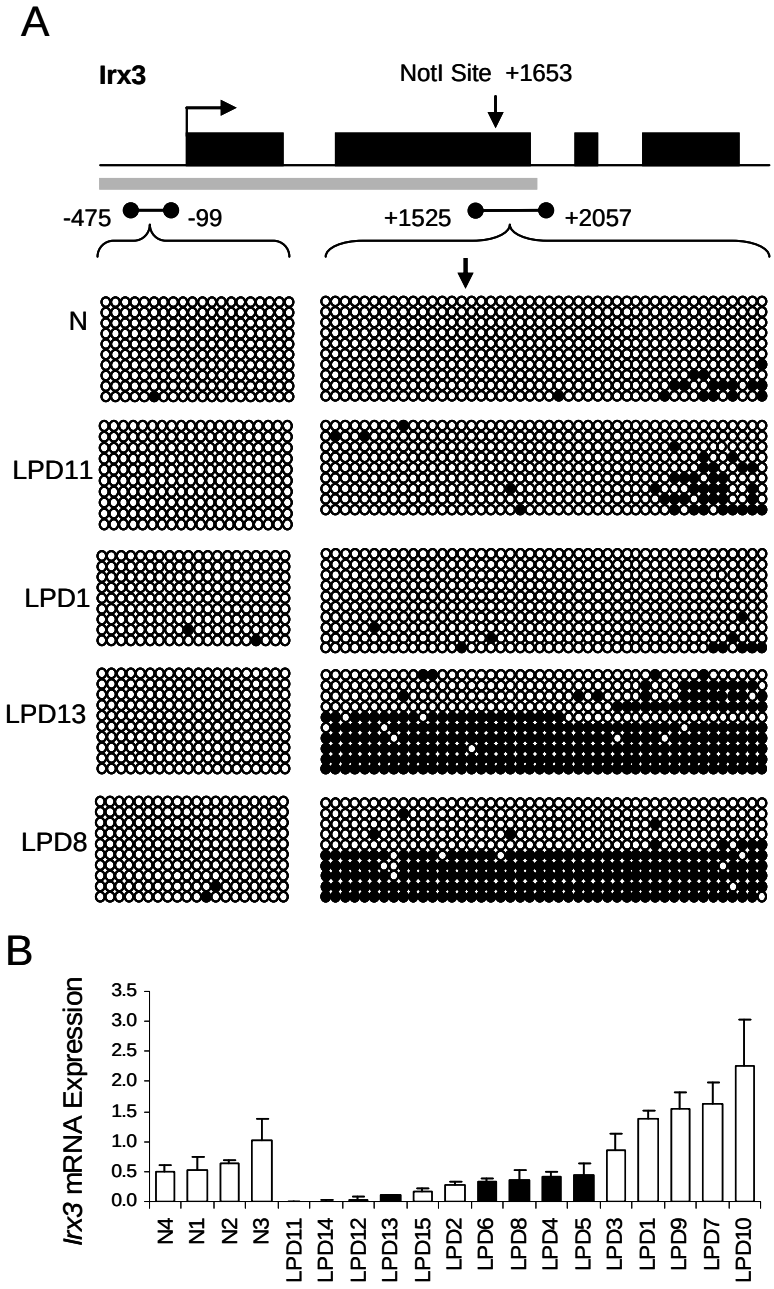

Figure 2. TRAMP tumors displaying downstream hypermethylation of the CDKN2A locus show increased mRNA expression of *p19* and *p16*. A-B) p19 and p16 mRNA expression in LPD, MET and AIP tumors grouped by either methylated or unmethylated RLGS status. † no AIP samples are unmethylated at this locus by RLGS analysis C-D) p19 and p16 mRNA expression in N, PIN, WD, EPD, and LPD samples. Mann-Whitney test p-values: ** $p < 0.005$; * $p < 0.01$, for each group compared to normal prostate.

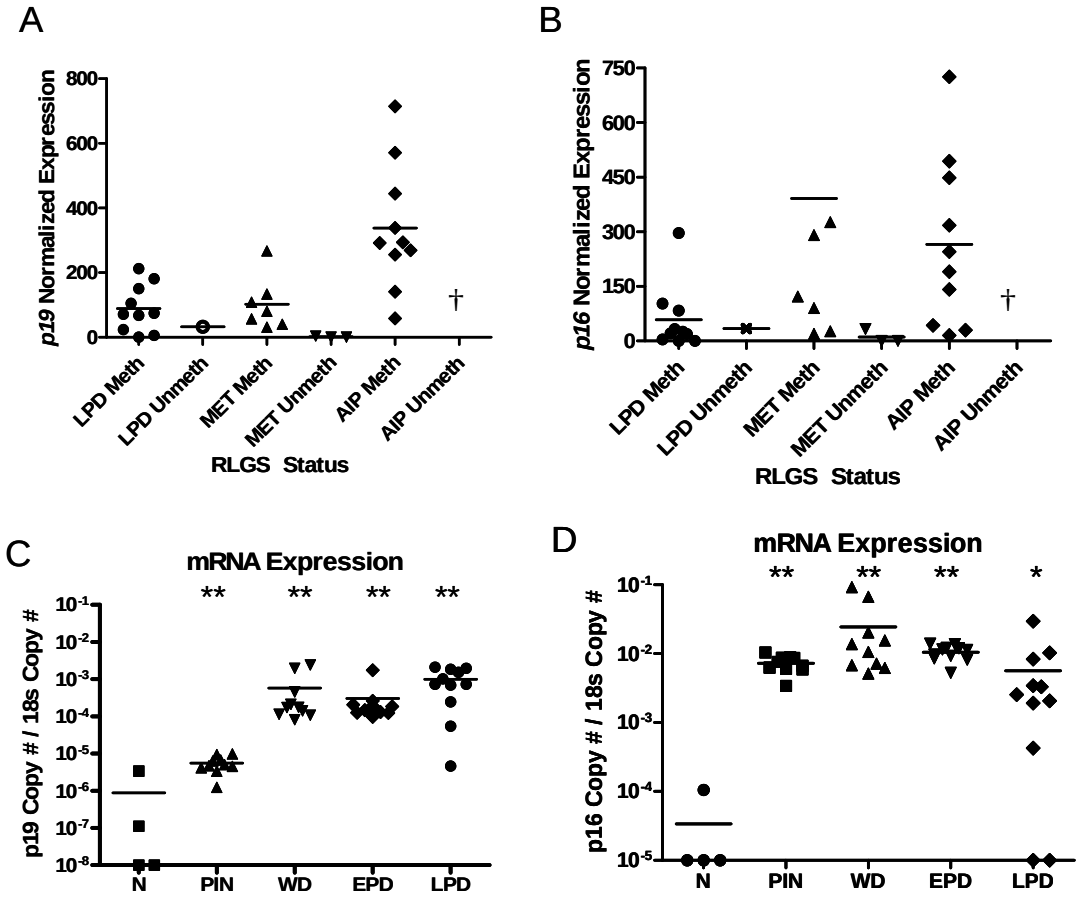

Figure 3. *p19* and *p16* expression are decreased in TRAMP C2D cell line with DAC treatment. A) *p19* and *p16* mRNA expression in TRAMP C2D cell line without and with DAC treatment for 48 hours. B) Bisulfite pyrosequencing analysis of the hypermethylated CDKN2A downstream region without and with DAC treatment in TRAMP C2D cell line.

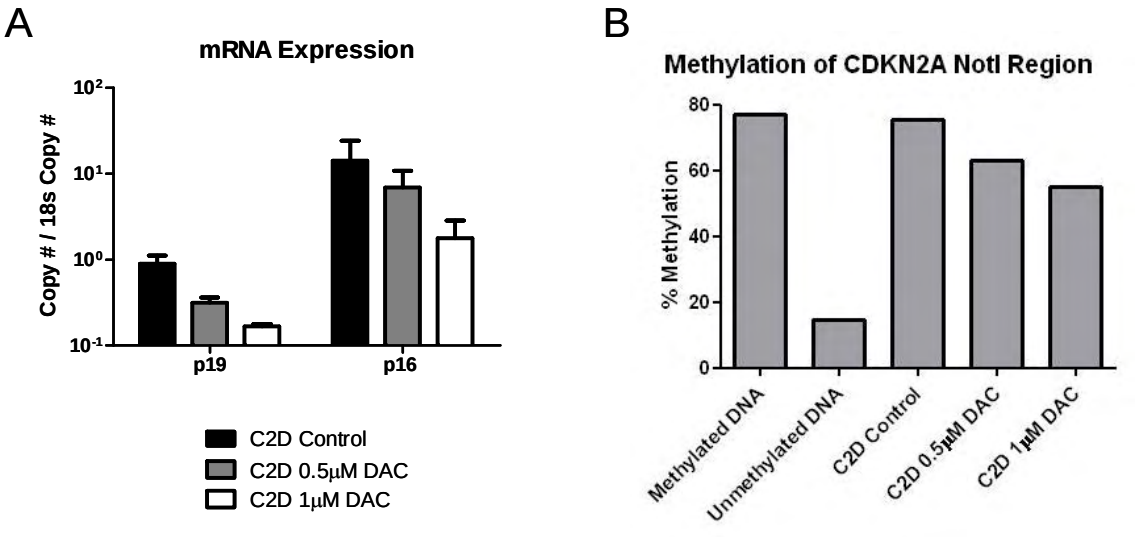

Figure 4. Bisulfite sequencing analysis of CDKN2A, Cacna1a, GSC and NRXN2 loci. A) Upper: diagram of the Cdkn2a locus. Open rectangles, p19 exons; hashed rectangles, p16 exons; lines, introns; right arrows, transcriptional start sites; vertical arrow, position of the NotI site identified by RLGS; black rectangles, CpG islands; horizontal line with circles (A-C), regions analyzed by sodium bisulfite sequencing. Lower: sodium bisulfite sequencing data of regions A-C in normal prostate and TRAMP samples. Percent methylation (averaged over the entire sequenced region), from at least ten sequenced clones per sample, is plotted. B) Upper: diagram of the Cacna1a locus. Right arrow, transcriptional start site; open rectangles, exons; lines, introns; vertical arrow, position of the NotI site identified by RLGS; black bar, CpG island; horizontal line with circles (A and B), regions analyzed by sodium bisulfite sequencing. Lower: sodium bisulfite sequencing data of regions A and B in normal prostate and TRAMP samples. Percent methylation (averaged over the sequenced entire region), from at least ten sequenced clones per sample, is plotted. C-D) MAQMA bisulfite sequencing results for the Gsc and Nrxn2 loci. Percent methylation (averaged over the sequenced entire region), plotted against sample type and RLGS methylation status.

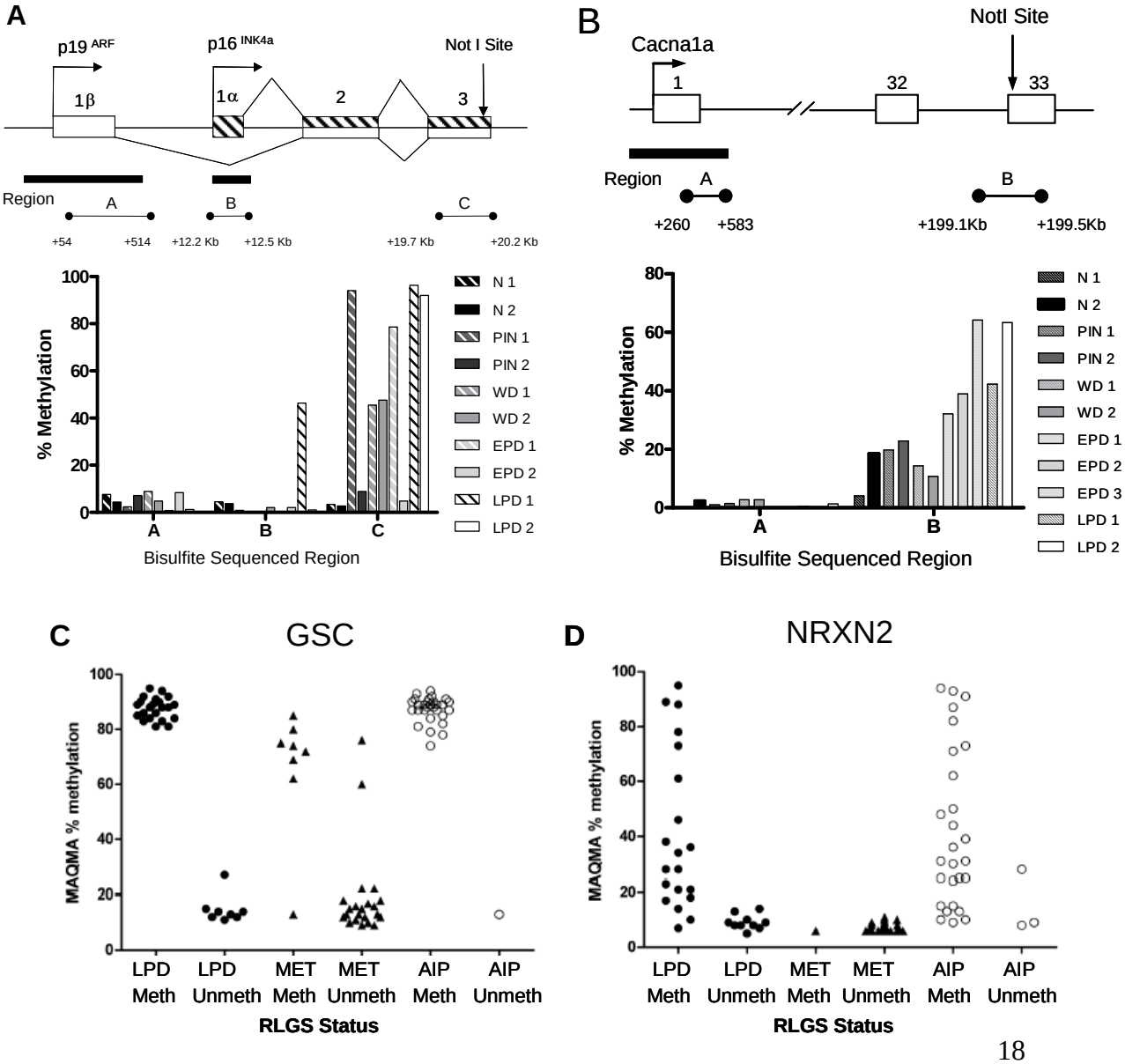

Table 3. Inheritance analysis of Dnmt1 hypomorphic alleles				
Genotype	WT	N/+	R/+	N/R
# Mice analyzed	53	46	49	8
Mendelian Ratio	1.1	0.9	1.0	0.2

Figure 5. Animal, urogenital (UG), and prostate weight in Dnmt1 hypomorphic mice. A) Weight of animal at sacrifice in Dnmt1 hypomorphic mice in all four genotypes (WT, N/+, R/+, N/R) at either 15 or 24 weeks of age. B) Urogenital weight at sacrifice in Dnmt1 hypomorphic mice in all four genotypes (WT, N/+, R/+, N/R) at either 15 or 24 weeks of age. C) Prostate weight at sacrifice in Dnmt1 hypomorphic mice in all four genotypes (WT, N/+, R/+, N/R) at either 15 or 24 weeks of age. Mann-Whitney test p-values: ** $p < 0.005$; * $p < 0.01$, for each group compared to WT for each time point.

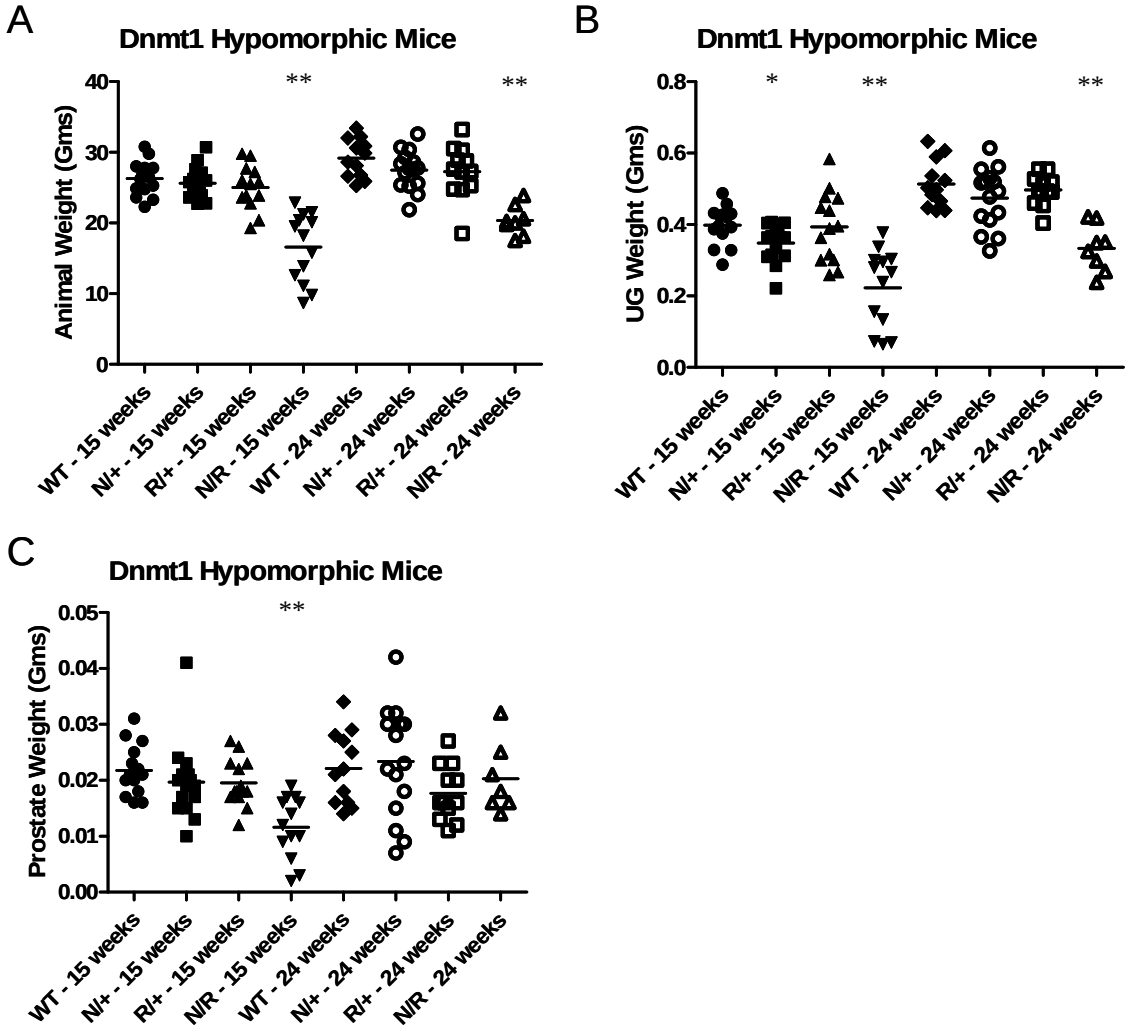

Figure 6. Global Methylation is decreased in Dnmt1 hypomorphic mice in both prostate and liver. A) Global methylation levels in prostate measured as %5mdC by liquid chromatography mass spectrometry in Dnmt1 hypomorphic mice in all four genotypes (WT, N/+, R/+, N/R) at either 15 or 24 weeks of age. B) Global methylation levels in liver measured as %5mdC by liquid chromatography mass spectrometry in Dnmt1 hypomorphic mice in all four genotypes (WT, N/+, R/+, N/R) at either 15 or 24 weeks of age. Mann-Whitney test p-value: * $p < 0.01$, for each group compared to WT for each time point.

A

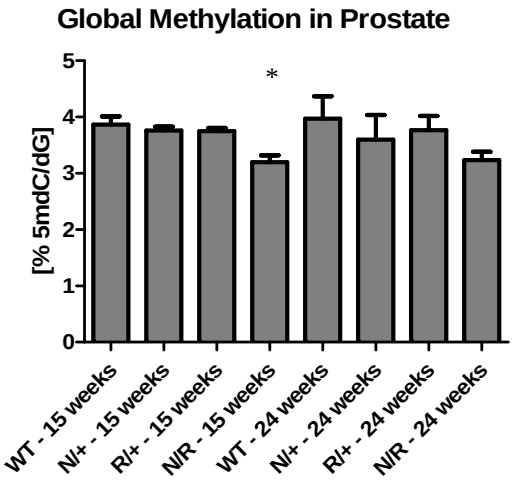

B

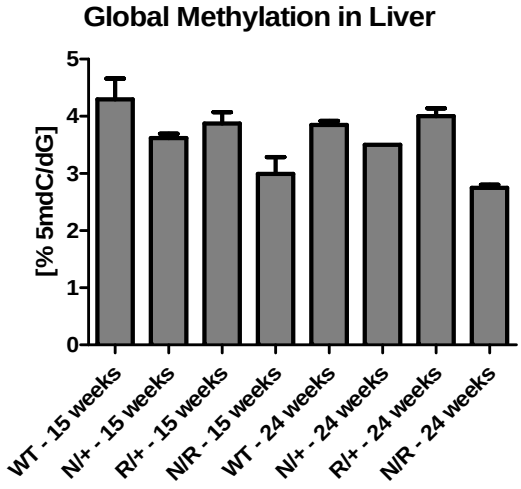

Figure 7. Animal, urogenital, and prostate weight in Dnmt1 Hypomorphic TRAMP mice. A) Weight of animal at sacrifice in Dnmt1 hypomorphic TRAMP mice in all three genotypes (WT, N/+, R/+) at either 15 or 24 weeks of age. B) Urogenital weight at sacrifice in Dnmt1 hypomorphic TRAMP mice in all three genotypes (WT, N/+, R/+) at either 15 or 24 weeks of age. C) Prostate weight at sacrifice in Dnmt1 hypomorphic TRAMP mice in all three genotypes (WT, N/+, R/+) at either 15 or 24 weeks of age. Mann-Whitney test p-value: * $p < 0.05$, for each group compared to WT for each time point.

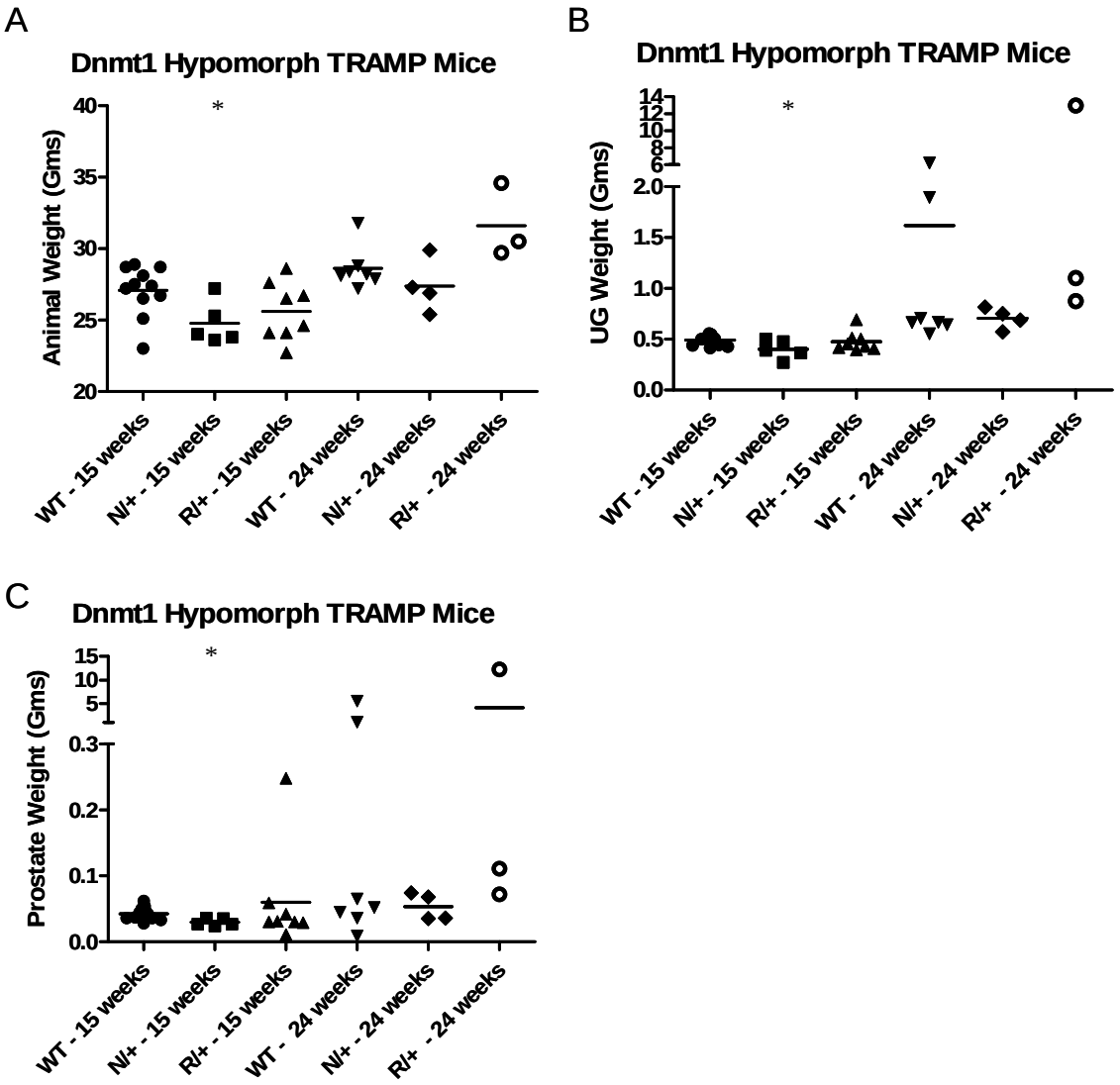

Publication 1:

Stage-specific alterations of Dnmt expression, DNA hypermethylation, and DNA hypomethylation during prostate cancer progression in the TRAMP model

Molecular Cancer Research. 2008. (In press)

Shannon R. Morey Kinney[1], Dominic J. Smiraglia[2], Smitha R. James[1], Michael T. Moser[1], Barbara A. Foster[1], and Adam R. Karpf[1]

Departments of Pharmacology and Therapeutics[1] and Cancer Genetics[2],
Roswell Park Cancer Institute, Elm and Carlton Streets, Buffalo, NY 14263.

Send Reprint Requests to: Dr. Adam R. Karpf, Department of Pharmacology & Therapeutics, Roswell Park Cancer Institute, Elm and Carlton Streets, Buffalo, NY 14263. Phone: 716-845-8305, e-mail: adam.karpf@roswellpark.org

Running title - Altered DNA methylation during TRAMP progression

Keywords - TRAMP, DNA methylation, epigenetics, prostate cancer, DNA methyltransferase

Grant Information: NIH R21CA128062 (ARK), NIH 5T32CA009072 (SRMK), DOD PC060354 (SRMK), NCI Center Grant CA16056 (Roswell Park Cancer Institute).

Abstract

We analyzed DNA methyltransferase protein expression and DNA methylation patterns during four progressive stages of prostate cancer in the *Transgenic Adenocarcinoma of Mouse Prostate* (TRAMP) model, including prostatic intraepithelial neoplasia (PIN), well differentiated tumors (WD), early poorly differentiated tumors (EPD), and late poorly differentiated tumors (LPD). Dnmt1, Dnmt3a, and Dnmt3b protein expression are increased in all stages, coinciding with overexpression of E2F gene targets, linking this alteration to Rb inactivation by Large T antigen. After normalization to Cyclin A to account for cell cycle regulation, Dnmt proteins remained over-expressed in all stages except LPD. Restriction Landmark Genomic Scanning (RLGS) analysis of locus-specific methylation revealed a high incidence of hypermethylation only in poorly differentiated (EPD and LPD) tumors. Several genes identified by RLGS showed hypermethylation of downstream regions correlating with mRNA overexpression, including *p16INK4a*, *p19ARF*, and *Cacna1a*. Parallel gene expression and DNA methylation analyses suggests that gene overexpression precedes downstream hypermethylation during prostate tumor progression. In contrast to gene hypermethylation, genomic DNA hypomethylation, including hypomethylation of repetitive elements and loss of genomic 5mdC, occurred in both early and late stages of prostate cancer. Statistical correlation analyses reveal that locus-specific hypermethylation and global hypomethylation are not associated in TRAMP. Notably, Dnmt1 and Dnmt3b over-expression correlated with global DNA hypomethylation, but

not locus-specific hypermethylation, suggesting the existence of a regulatory loop responsive to global DNA hypomethylation that involves specific Dnmts. In summary, our data reveal the temporal relationship between key alterations of the DNA methylation pathway occurring during prostate tumor progression.

Introduction

DNA methylation is deregulated in cancer such that the promoter regions of tumor suppressor genes become hypermethylated, resulting in gene silencing, while, on a global level, DNA becomes hypomethylated, potentially leading to genomic instability (4, 5). In human prostate cancer, both of these mechanisms have been observed (6). In addition, deregulated expression of DNA methyltransferase (Dnmt) proteins is seen in human prostate cancer . These data provide compelling circumstantial evidence of a role for these alterations in prostate cancer development. However, it is difficult to assess the functional contribution of these alterations to prostate cancer development using only human clinical samples. Moreover, the relative timing of and relationship between distinct DNA methylation pathway alterations during prostate tumor progression has not been assessed in an experimentally tractable model system. To this end, we and others have recently established TRAMP (*Transgenic Adenocarcinoma of Mouse Prostate*) as a suitable mouse model to investigate the role of altered DNA methylation in prostate cancer development (2, 7, 8). We have shown that late stage primary tumors and metastases from TRAMP mice display increased Dnmt expression, locus-specific non-random CpG island hypermethylation, and hypomethylation of repetitive DNA elements (2). In addition, others have demonstrated, using pharmacological inhibition of Dnmt enzymes, that DNA hypermethylation contributes to the development of primary cancer in both intact and castrated TRAMP mice (7, 8). Taken together, these data suggest that the TRAMP model may be particularly useful to clarify the role of DNA methylation pathway alterations in prostate cancer development.

One notable finding of our previous study was that TRAMP tumors frequently display overexpression of *p19ARF* (p19) and *p16INK4a* (p16), correlating with hypermethylation of a shared downstream region (exon 3) of the Cdkn2a locus (2). The relevance of this event to human prostate cancer is supported by the prior observation that p16 gene up-regulation and downstream hypermethylation also occur in human prostate cancer . Using Restriction Landmark Genomic Scanning (RLGS), we identified several other genes that were hypermethylated in downstream regions in TRAMP, relative to normal prostate, suggesting that this phenomenon may be widespread (2). Previous work in other systems has also reported hypermethylation of actively transcribed downstream gene regions in cancer . However, it remains unclear whether gene overexpression in cancer occurs prior or subsequent to downstream DNA hypermethylation.

In the current study we sought to define the relationship between disease stage, Dnmt expression, DNA hypermethylation, and DNA hypomethylation in prostate cancer. For this purpose, we selected TRAMP prostate samples from four distinct groups (prostatic intraepithelial neoplasia (PIN), well-differentiated tumors (WD), early poorly differentiated tumors (EPD), and late poorly differentiated tumors (LPD)) for analysis, for comparison to non-transgenic strain matched normal mouse prostates. In each sample set we measured Dnmt1, Dnmt3a, and Dnmt3b protein expression by Western blot, locus-specific methylation using RLGS, and global methylation using Liquid

Chromatography-Mass Spectrometry (LC-MS) detection of 5-methyldeoxycytidine (5mdC), and bisulfite pyrosequencing of the B1 repetitive element. In addition, we examined the relationship between gene overexpression and downstream hypermethylation in TRAMP, via comparative mRNA expression and DNA methylation analysis of p16INK4a, p19ARF, and Cacna1a in staged tumor samples. Importantly, we performed statistical correlation analyses to assess the relationship between each of these parameters during tumor progression. Our findings reveal key aspects of the relationship between distinct alterations of the DNA methylation pathway occurring during prostate tumor progression.

Results

Multi-stage Prostate Cancer (CaP) Progression in TRAMP. In this study, we utilized prostate tumors from TRAMP mice, as well as normal prostates from non-transgenic, strain-matched mice (Fig. 1A). We grouped TRAMP samples based on differentiation status, age, and prostate weight into the following four categories: Prostatic Intraepithelial Neoplasia (PIN, 10-12 weeks, 0.008-0.04 gm, n = 35), well-differentiated tumors (WD, 15-20 weeks, 0.03-0.09 gm, n = 25), early poorly-differentiated tumors (EPD, 15-20 weeks, 0.49-4.86 gm, n = 12), and late poorly-differentiated tumors (LPD, 22-28 weeks, 1.65-15-65 gm, n = 12) (Fig. 1A). This grouping is based on previous studies showing that age and prostate weight directly correlate with tumor progression in TRAMP (9). PIN samples are normal in weight, but microscopically display neoplasia and hyperplastic infolding of the epithelial layer into the luminal space of the gland (Fig. 1, A and B). WD samples are larger than normal prostates, but were not palpable at necropsy. The majority of the disease in these samples is well differentiated glandular epithelium (Fig. 1B). EPD samples are from the same age range as WD samples (15-20 weeks), but were palpable at necropsy and histologically demonstrated predominantly sheets of poorly differentiated epithelial cells (Fig. 1, A and B). LPD tumors, from 20-28 week old mice, were very large and show poorly differentiated late stage disease (Fig. 1, A and B). Hematoxylin and eosin (H&E) staining was used to stage a subset of samples and confirmed the assigned groupings (Fig. 1B and data not shown).

Dnmt protein expression during multi-stage CaP progression. We initially examined Dnmt1, Dnmt3a, and Dnmt3b protein expression in normal prostates and the four sets of TRAMP samples described above using Western blot analysis. Dnmt1 expression is significantly elevated in PIN and WD and its level increases further in late stage (EPD and LPD) samples (Fig. 2A and B). Dnmt3a and Dnmt3b also show elevated expression in PIN and WD, which increases in EPD and LPD tumors (Fig. 2A, C-D). We measured Cyclin A, to normalize Dnmt expression, as Dnmt expression is cell cycle regulated with high level expression restricted to S phase . Cyclin A expression is robustly increased only in late stage (EPD and LPD) disease (Fig. 2A and E). As expected based on our previous work, there was a strong association between the expression of each Dnmt and the expression of Cyclin A, SV40 Large T antigen and E2F1 (and data not shown). Notably, after normalization to Cyclin A, Dnmt1 and Dnmt3b expression are significantly upregulated in PIN, WD, and EPD, but no longer in LPD tumors (Fig. 2F and H). Dnmt3a is upregulated only in PIN and WD tumors after normalization to Cyclin A (Fig. 2G). Taken together, these data indicate that increased

Dnmt protein expression is not solely accounted for by increased cell proliferation, and may be most biologically significant at early progression stages in TRAMP.

Locus-specific DNA hypermethylation during multi-stage CaP progression. We next utilized RLGS to examine global CpG island methylation patterns in TRAMP samples of each progression stage. RLGS is a two-dimensional gel analysis of radio-labeled, methylation sensitive enzyme-restricted DNA fragments . When comparing RLGS gel patterns, spot loss and spot gain correspond to DNA hypermethylation and DNA hypomethylation events, respectively. RLGS allowed for the identification of hypermethylation events in TRAMP which, in the vast majority of instances, were confined to late stage (EPD or LPD) disease (examples shown in Fig. 3A and B). A low level of both hypermethylation and hypomethylation events were observed in PIN and WD samples, while EPD and LPD tumors showed a substantial increase in hypermethylation events (Fig. 3C and D). In addition, the number of hypermethylated loci from tumor to tumor was variable within the EPD, and particularly the LPD, groups (Fig. 3D). We identified the genes corresponding to different RLGS spots using cloning techniques described previously (Table 1). A number of these loci were hypermethylated at high frequency in EPD and LPD (Table 1), suggesting that methylation of these loci are under positive selection during prostate cancer progression in TRAMP.

Downstream hypermethylation and increased gene expression. We previously reported that overexpression of *p19* and *p16* correlated with the downstream hypermethylation at the shared exon 3 of the Cdkn2a locus in late stage TRAMP tumors (2). Several other genes also display hypermethylation in downstream regions in TRAMP tumors, providing further evidence of the potential importance of this phenomenon (Table 1, genes in bold). The staged progression model we describe here allows for an investigation of the relative timing of gene overexpression and downstream hypermethylation. We find that *p19* and *p16* are over-expressed in all stages analyzed, as compared to normal prostate, indicating that overexpression is an early event (Fig. 4A and B). In contrast, RLGS indicated that hypermethylation of the NotI site at exon 3 of the Cdkn2a locus was exclusively found in late stage (EPD and LPD) samples (Table 1). Bisulfite sequencing confirmed that TRAMP tumors sometimes fail to show Cdkn2a exon 3 hypermethylation, despite the fact that overexpression is uniformly observed in these lesions (Fig. 4C). These data suggest that gene overexpression precedes downstream hypermethylation at the Cdkn2a locus during tumor progression. Moreover, downstream hypermethylation at the Cdkn2a locus in TRAMP is rarely accompanied by hypermethylation at the p19 or p16 promoter regions (Fig. 4C).

To investigate this phenomenon at a distinct locus, we measured the expression and methylation of the calcium channel gene *Cacna1a,* which is frequently methylated in a 3' region (exon 33) in TRAMP (Table 1). Cacna1a is overexpressed only in late stage (EPD and LPD) tumors, paralleling its exclusive methylation in these stages (Fig. 5A, Table 1). Notably, overexpression occurred in all analyzed late stage (EPD and LPD) samples, while downstream hypermethylation occurred only in approximately half of these samples (Fig. 5A, Table 1). Bisulfite sequencing further demonstrated that this downstream region of Cacna1a, but not its promoter region, is methylated in TRAMP (Fig. 5B). Taken together, these data suggest that, similar to Cdkn2a genes, overexpression of Cacna1a precedes its downstream hypermethylation. Interestingly, a low but significant level of methylation at the Cacna1a locus was seen in both normal

prostates and early stage samples (Fig. 5B). This situation may be analogous to certain genes that are partially methylated in normal human prostate and become hypermethylated in human prostate cancer .

DNA hypomethylation during multi-stage CaP progression. In addition to gene specific DNA hypermethylation, global DNA hypomethylation appears to contribute to oncogenesis . In TRAMP, we previously found increased variability but no consistent changes in 5mdC levels in late stage TRAMP tumors and metastases as compared to normal strain-matched prostates (2). We hypothesized that global hypomethylation may be an early event during TRAMP tumor development that could have been missed in our previous study. To test this hypothesis, we measured 5mdC levels by LC-MS as well as the methylation level of the common murine repetitive element B1 using quantitative bisulfite pyrosequencing, in the four stages of TRAMP samples described earlier (Fig 1A). Notably, 5mdC levels were significantly decreased in WD and EPD tumors (Fig. 6A). At the latest stage, LPD, this effect was lost; however increasing variability from tumor to tumor was apparent (Fig 6A). In contrast to 5mdC levels, the B1 repetitive element is significantly hypomethylated in all four progression stages measured, but more dramatically in the later stages (Fig. 6B). Analyzed over the entire data set, 5mdC levels directly correlated with B1 methylation (Spearman Rank Correlation $r = 0.30$, $p=0.04$). These experiments demonstrate that genomic DNA hypomethylation occurs as an early event during prostate tumorigenesis in TRAMP, and persists and/or increases in advanced stages.

Relationship between DNA methylation pathway alterations in TRAMP. We took advantage of our unique data set to examine the relationship between Dnmt protein expression, DNA hypermethylation, and DNA hypomethylation during prostate tumorigenesis. To examine the potential link between DNA hypermethylation and DNA hypomethylation, we compared the extent of RLGS spot loss to 5mdC levels or B1 element methylation status in all samples (Fig. 6C and D). Notably, there was no association between DNA hypermethylation and either parameter of global DNA hypomethylation, suggesting that hyper- and hypomethylation are independently controlled in TRAMP. The lack of association was still seen when only late stage (EPD and LPD) samples, which show a much higher incidence of DNA hypermethylation (Fig 3), were analyzed (Fig. 6E and F).

We also compared Dnmt1, Dnmt3a, and Dnmt3b protein expression, after normalization to Cyclin A, to DNA hypermethylation and DNA hypomethylation. Dnmt protein expression did not correlate with RLGS spot loss (DNA hypermethylation) in all TRAMP samples, suggesting that locus-specific DNA hypermethylation may result from a defect in methylation targeting rather than from altered Dnmt expression (Table 2). Again, a lack of association between these parameters was maintained when only late stage tumors (EPD and LPD) were analyzed (data not shown). Interestingly, expression of Dnmt1 and Dnmt3b, but not Dnmt3a, was inversely correlated with 5mdC levels (Table 2). For B1 methylation, the same trend was apparent, but did not reach statistical significance (Table 2). This intriguing finding suggests that Dnmt1 and Dnmt3b protein overexpression in prostate cancer may reflect a regulatory loop responsive to global DNA hypomethylation.

Discussion

We have utilized the TRAMP model to elucidate the nature and the temporal relationship of distinct DNA methylation pathway alterations occurring during prostate cancer development. A unified model encompassing the data presented here, as well that of our previous work , is shown in Fig 7. At the earliest stage analyzed, PIN, a number of alterations are already detected, including Dnmt protein overexpression, hypomethylation of the B1 repetitive DNA element and, to a lesser extent, gene-specific DNA hypermethylation (Fig. 7). 5mdC loss is substantial at the WD and EPD stages, but becomes highly heterogeneous later on (Fig. 7). DNA hypermethylation becomes highly prevalent only in late stage primary and metastatic tumors (Fig. 7). Similar to the heterogeneous 5mdC levels seen in late progression stages, there is increased heterogeneity of DNA hypermethylation events in metastatic lesions (Fig. 7).

Unexpectedly, correlation analyses indicate that Dnmt1 and Dnmt3b protein overexpression is directly associated with DNA hypomethylation, but not with DNA hypermethylation. At first, this finding appears counterintuitive. However, these data could be explained if Dnmt1 and Dnmt3b protein overexpression is driven by a feedback mechanism involving detection of global 5mdC loss (Fig. 7, dashed line). It will be crucial to investigate this potential regulatory circuit in future studies. A lack of association between Dnmt overexpression and DNA hypermethylation is consistent with studies of ovarian and lung cancer , and suggests that improper targeting of Dnmt proteins to specific loci, or positive selection of stochastic hypermethylation events, rather than increased Dnmt expression, drives locus-specific DNA hypermethylation in prostate cancer. The former model is in agreement with previous studies showing that specific DNA motifs have an intrinsic propensity for aberrant DNA hypermethylation .

In TRAMP, accumulating evidence suggests that aberrant DNA hypermethylation directly contributes to the disease progression. Treatment of TRAMP mice with the Dnmt inhibitor DAC delays tumor progression, without altering the incidence of early stage disease (7). Consistent with this finding, we observe that very few aberrant locus specific hypermethylation events are detected in early stage tumors (PIN and WD), while a large number of these events are seen in late stage tumors (EPD and LPD). The fact that high frequency gene specific DNA hypermethylation occurs only at late stages of prostate cancer suggests that they may result from tumor selection and not simply transgene expression. This is in agreement with a recent study examining DNA hypermethylation in a murine lymphoma model, which found changes in DNA methylation only in late stage disease (10).

In TRAMP, increased expression of *p19* and *p16* occur as early as the PIN stage while overexpression of *Cacna1a* occurs at later stage disease. For each gene, increased expression coincides with regional downstream DNA hypermethylation. It is intriguing that downstream hypermethylation of overexpressed genes occurs at several loci in TRAMP (Table 1). The relative timing of these two events *in vivo*, for the genes studied here, suggests that gene overexpression occurs prior to and may facilitate downstream hypermethylation. However, in preliminary studies we have observed that treatment of TRAMP cell lines with DNA methyltransferase inhibitor 5-aza-2'-deoxyctidine results in decreased expression of *p19* and *p16*, coinciding with reduced downstream hypermethylation (data not shown). Taken together, these data appear to suggest that increased transcription facilitates downstream hypermethylation, which may then

contribute to the maintenance of the transcriptionally active state. In vivo manipulation of DNA methylation levels in TRAMP mice will be required to adequately test this hypothesis. In any case, it is important to point out that *p16* gene expression is also increased in human prostate cancer, in conjunction with hypermethylation of downstream regions , strongly supporting the relevance of our observations in the TRAMP model.

Significant reduction of global 5mdC occurs only in the WD and EPD stages; in contrast, the B1 element is hypomethylated at all stages, including PIN. This result suggests that DNA hypomethylation of certain genomic regions is a very early event during prostate tumor progression but is not uniform across the entire methylome. Notably, locus-specific hypermethylation and global genomic hypomethylation did not correlate, suggesting that the two events make independent contributions to prostate cancer development. In the context of murine intestinal tumorigenesis, Jaenisch and colleagues have shown that DNA hypomethylation accelerates the formation of early stage microadenomas, but dramatically inhibits the formation of macroscopic polyps . Our findings suggest that an analogous scenario could occur in murine prostate cancer, with hypomethylation contributing to tumor initiation and hypermethylation contributing to tumor progression. The increased heterogeneity of both hypo- and hypermethylation in late stage prostate disease in TRAMP suggests a general decrease in the fidelity of DNA methylation in these tumors, which may serve as a source of tumor heterogeneity.

In summary, we have utilized a progression stage model of prostate cancer to decipher the temporal relationship between the three chief DNA methylation pathway alterations in cancer. Key aspects of this model will allow for the examination of the role of specific epigenetic defects to prostate tumor development *in vivo*.

Materials and Methods

Animals and tissue samples. Fig. 1A summarizes the TRAMP samples used in this study. Normal prostate samples were obtained from f1 males generated by crosses of C57BL/6 and FVB strain mice. TRAMP prostate tissues were obtained from f1 males generated by crosses of C57BL/6 TRAMP males (homozygous for the Probasin-SV40 transgene) with wildtype FVB females. Thus, all TRAMP tumors were heterozygous for the transgene. All prostate and tumor tissues were microdissected at necropsy. Samples were flash frozen in liquid nitrogen, and stored at -80^0C until use.

Hematoxylin and Eosin (H&E) Staining. Five micron thick tissue sections were cut from paraffin embedded blocks and mounted on slides. Slides were deparafinized and rehydrated with Xylene and graded alcohol and equilibrated with Tris-phosphate buffer. Samples were then stained with H&E, dehydrated through alcohol into xylene, and mounted with glass coverslips. Tissue sections were scored using a compound Olympus XI-50 microscope equipped with QCapture imaging software.

Western blot analysis. Nuclear proteins were extracted from mouse tissues using the Nuclear Extract kit (Pierce Biochemical, Rockland, IL). Protein concentrations were determined using the Lowry High system (BioRad, Hercules, CA). Western blots were completed as described previously (2). Dnmt1 was detected using the NB 100-264 rabbit polyclonal antibody (Novus Biologicals, Littleton CO). Dnmt3a was detected with ab14291 chicken polyclonal antibody (Abcam Inc., Cambridge, MA). Dnmt3B was detected using the NB 100-266 rabbit polyclonal antibody (Novus Biologicals). Cyclin A and E2F1 were detected using the sc-751 and sc-193 rabbit polyclonal antibodies,

respectively (Santa Cruz Biotechnology, Santa Cruz, CA) and Tag was detected with monoclonal mouse SV-40 large T antigen antibody 554149 (BD Pharmingen, San Diego, CA). Band density was analyzed using the Personal Densitometer SI instrument and ImageQuant 5.2 software (Molecular Dynamics, Sunnyvale, CA).

Restriction Landmark Genomic Scanning (RLGS) and RLGS spot cloning. High molecular weight genomic DNA was isolated from TRAMP samples and non-transgenic control prostates as described previously . Individual tumor samples (~75 mg of tissue) were used for DNA isolation and RLGS analysis. Normal prostate samples were segregated into four pools of 3-4 prostates to allow for isolation of sufficient high molecular weight DNA for RLGS. RLGS was performed as described previously . Hypermethylated genes in TRAMP were identified by RLGS spot cloning as described previously .

Quantitative Reverse Transcriptase PCR (qRT-PCR). RNA samples were extracted from mouse tissues and converted to cDNA as described previously . PCR reactions were conducted using qPCR SYBR MasterMix (Eurogentec, San Diego, CA) and the 7300 Real Time PCR System (Applied Biosystems, Foster City, CA). Primer sequences for analysis of *p19, p16, Cacna1a* and *18s rRNA* expression were designed using the Primer3 web-based program and are available upon request. SYBR green absolute quantification analysis was used to determine target gene copy number, which was normalized to *18s rRNA*.

Sodium Bisulfite Sequencing. Genomic DNAs were isolated using the Puregene kit (Gentra Systems) and sodium bisulfite conversion was performed using the EZ DNA Methylation Kit (Zymo Research). Sodium bisulfite sequencing primers were designed using *MethPrimer* and are available upon request. Gradient PCR reactions were used to optimize annealing temperatures for each primer set. PCR products were directly cloned into the pTopoTA 4.1 vector (Invitrogen, Carlsbad, CA) and individual clones were sequenced at the RPCI Biopolymer core facility, using an ABI prism automated DNA sequencer. DNA sequence information was analyzed using Lasergene (DNASTAR Inc., Madison, WI). A minimum of 10 independent clones were sequenced per sample.

Determination of 5mdC levels. 5mdC levels were determined using liquid chromatography-electrospray ionization quadrapole mass spectrometry (LC-MS) as described previously . Genomic DNAs were isolated using the Puregene DNA isolation kit (Gentra Systems) and 1 μg genomic DNA samples were digested using 4 units of Nuclease S1 (Fermentas). All samples were analyzed in duplicate.

B1 Repetitive Element Pyrosequencing. Genomic DNA isolation and sodium bisulfite conversion were completed as described above. A bisulfite pyrosequencing assay for the murine B1 element was performed as described previously , with slight modifications. The pyrosequencing primer (CpG 2) was utilized (11). Pyrosequencing of the purified single-stranded PCR product was accomplished using the PSQ HS96 Pyrosequencing System (Biotage AB, Uppsala, Sweden). The sequence analyzed contains 2 CpG sites (5'-CGAACTCAGAAATCCG-3') and the mean methylation value of both sites was averaged for each sample. All samples were analyzed in duplicate.

References

1. Camoriano, M., Shannon R. Morey Kinney, Michael T. Moser, Barbara A. Foster, James L. Mohler, Donald L. Trump, Adam R. Karpf, and Dominic J. Smiraglia. Phenotype-specific CpG Island Methylation Events in a Murine Model of Prostate Cancer. Cancer Research, *In Press*, 2008.
2. Morey, S. R., Smiraglia, D. J., James, S. R., Yu, J., Moser, M. T., Foster, B. A., and Karpf, A. R. DNA methylation pathway alterations in an autochthonous murine model of prostate cancer. Cancer Res, *66:* 11659-11667, 2006.
3. Morey Kinney, S. R., Dominic J. Smiraglia, Smitha R. James, Michael T. Moser, Barbara A. Foster, and Adam R. Karpf Stage-specific alterations of Dnmt expression, DNA hypermethylation, and DNA hypomethylation during prostate cancer progression in the TRAMP model. Molecular Cancer Research, *In Press*, 2008.
4. Feinberg, A. P. and Tycko, B. The history of cancer epigenetics. Nat Rev Cancer, *4:* 143-153, 2004.
5. Jones, P. A. and Baylin, S. B. The fundamental role of epigenetic events in cancer. Nat Rev Genet, *3:* 415-428, 2002.
6. Kang, G. H., Lee, S., Lee, H. J., and Hwang, K. S. Aberrant CpG island hypermethylation of multiple genes in prostate cancer and prostatic intraepithelial neoplasia. J Pathol, *202:* 233-240, 2004.
7. McCabe, M. T., Low, J. A., Daignault, S., Imperiale, M. J., Wojno, K. J., and Day, M. L. Inhibition of DNA methyltransferase activity prevents tumorigenesis in a mouse model of prostate cancer. Cancer Res, *66:* 385-392, 2006.
8. Zorn, C. S., Wojno, K. J., McCabe, M. T., Kuefer, R., Gschwend, J. E., and Day, M. L. 5-aza-2'-deoxycytidine delays androgen-independent disease and improves survival in the transgenic adenocarcinoma of the mouse prostate mouse model of prostate cancer. Clin Cancer Res, *13:* 2136-2143, 2007.
9. Kaplan-Lefko, P. J., Chen, T. M., Ittmann, M. M., Barrios, R. J., Ayala, G. E., Huss, W. J., Maddison, L. A., Foster, B. A., and Greenberg, N. M. Pathobiology of autochthonous prostate cancer in a pre-clinical transgenic mouse model. Prostate, *55:* 219-237, 2003.
10. Opavsky, R., Wang, S. H., Trikha, P., Raval, A., Huang, Y., Wu, Y. Z., Rodriguez, B., Keller, B., Liyanarachchi, S., Wei, G., Davuluri, R. V., Weinstein, M., Felsher, D., Ostrowski, M., Leone, G., and Plass, C. CpG island methylation in a mouse model of lymphoma is driven by the genetic configuration of tumor cells. PLoS Genet, *3:* 1757-1769, 2007.
11. Jeong, K. S. and Lee, S. Estimating the total mouse DNA methylation according to the B1 repetitive elements. Biochem Biophys Res Commun, *335:* 1211-1216, 2005.
12. Nelson, W. G., De Marzo, A. M., and Isaacs, W. B. Prostate cancer. N Engl J Med, *349:* 366-381, 2003.
13. Byar, D. P. Proceedings: The Veterans Administration Cooperative Urological Research Group's studies of cancer of the prostate. Cancer, *32:* 1126-1130, 1973.
14. Labrie, F., Belanger, A., Dupont, A., Luu-The, V., Simard, J., and Labrie, C. Science behind total androgen blockade: from gene to combination therapy. Clin Invest Med, *16:* 475-492, 1993.

15. Baylin, S. B., Herman, J. G., Graff, J. R., Vertino, P. M., and Issa, J. P. Alterations in DNA methylation: a fundamental aspect of neoplasia. Adv Cancer Res, *72:* 141-196, 1998.
16. Gama-Sosa, M. A., Wang, R. Y., Kuo, K. C., Gehrke, C. W., and Ehrlich, M. The 5-methylcytosine content of highly repeated sequences in human DNA. Nucleic Acids Res, *11:* 3087-3095., 1983.
17. Costello, J. F. and Plass, C. Methylation matters. J Med Genet, *38:* 285-303, 2001.
18. Jones, P. A. Cancer. Death and methylation. Nature, *409:* 141, 143-144., 2001.
19. Laird, P. W. The power and the promise of DNA methylation markers. Nat Rev Cancer, *3:* 253-266, 2003.
20. Salem, C. E., Markl, I. D., Bender, C. M., Gonzales, F. A., Jones, P. A., and Liang, G. PAX6 methylation and ectopic expression in human tumor cells. Int J Cancer, *87:* 179-185, 2000.
21. Nguyen, C., Liang, G., Nguyen, T. T., Tsao-Wei, D., Groshen, S., Lubbert, M., Zhou, J. H., Benedict, W. F., and Jones, P. A. Susceptibility of nonpromoter CpG islands to de novo methylation in normal and neoplastic cells. J Natl Cancer Inst, *93:* 1465-1472, 2001.
22. Smith, J. F., Mahmood, S., Song, F., Morrow, A., Smiraglia, D., Zhang, X., Rajput, A., Higgins, M. J., Krumm, A., Petrelli, N. J., Costello, J. F., Nagase, H., Plass, C., and Held, W. A. Identification of DNA Methylation in 3' Genomic Regions that are Associated with Upregulation of Gene Expression in Colorectal Cancer. Epigenetics, *2,* 2007.
23. Verma, M. and Srivastava, S. Epigenetics in cancer: implications for early detection and prevention. Lancet Oncol, *3:* 755-763, 2002.
24. Smiraglia, D. J. and Plass, C. The development of CpG island methylation biomarkers using restriction landmark genomic scanning. Ann N Y Acad Sci, *983:* 110-119, 2003.
25. Harden, S. V., Guo, Z., Epstein, J. I., and Sidransky, D. Quantitative GSTP1 methylation clearly distinguishes benign prostatic tissue and limited prostate adenocarcinoma. J Urol, *169:* 1138-1142, 2003.
26. Jeronimo, C., Usadel, H., Henrique, R., Oliveira, J., Lopes, C., Nelson, W. G., and Sidransky, D. Quantitation of GSTP1 methylation in non-neoplastic prostatic tissue and organ-confined prostate adenocarcinoma. J Natl Cancer Inst, *93:* 1747-1752, 2001.
27. Lodygin, D., Epanchintsev, A., Menssen, A., Diebold, J., and Hermeking, H. Functional Epigenomics Identifies Genes Frequently Silenced in Prostate Cancer. Cancer Res, *65:* 4218-4227, 2005.
28. Wu, M. and Ho, S. M. PMP24, a gene identified by MSRF, undergoes DNA hypermethylation-associated gene silencing during cancer progression in an LNCaP model. Oncogene, *23:* 250-259, 2004.
29. Smiraglia, D. J., Rush, L. J., Fruhwald, M. C., Dai, Z., Held, W. A., Costello, J. F., Lang, J. C., Eng, C., Li, B., Wright, F. A., Caligiuri, M. A., and Plass, C. Excessive CpG island hypermethylation in cancer cell lines versus primary human malignancies. Hum Mol Genet, *10:* 1413-1419., 2001.

30. Greenberg, N. M., DeMayo, F., Finegold, M. J., Medina, D., Tilley, W. D., Aspinall, J. O., Cunha, G. R., Donjacour, A. A., Matusik, R. J., and Rosen, J. M. Prostate cancer in a transgenic mouse. Proc Natl Acad Sci U S A, *92:* 3439-3443, 1995.
31. Gingrich, J. R., Barrios, R. J., Morton, R. A., Boyce, B. F., DeMayo, F. J., Finegold, M. J., Angelopoulou, R., Rosen, J. M., and Greenberg, N. M. Metastatic prostate cancer in a transgenic mouse. Cancer Res, *56:* 4096-4102, 1996.
32. Eng, M. H., Charles, L. G., Ross, B. D., Chrisp, C. E., Pienta, K. J., Greenberg, N. M., Hsu, C. X., and Sanda, M. G. Early castration reduces prostatic carcinogenesis in transgenic mice. Urology, *54:* 1112-1119, 1999.
33. Gingrich, J. R., Barrios, R. J., Kattan, M. W., Nahm, H. S., Finegold, M. J., and Greenberg, N. M. Androgen-independent prostate cancer progression in the TRAMP model. Cancer Res, *57:* 4687-4691, 1997.
34. Mohler, J. L., Gregory, C. W., Ford, O. H., 3rd, Kim, D., Weaver, C. M., Petrusz, P., Wilson, E. M., and French, F. S. The androgen axis in recurrent prostate cancer. Clin Cancer Res, *10:* 440-448, 2004.
35. Berthon, P., Dimitrov, T., Stower, M., Cussenot, O., and Maitland, N. J. A microdissection approach to detect molecular markers during progression of prostate cancer. Br J Cancer, *72:* 946-951, 1995.
36. Smiraglia, D. J., Frühwald, M. C., Costello, J. F., McCormick, S. P., Dai, Z., Peltomäki, P., MS, O. D., Cavenee, W. K., and Plass, C. A New Tool for the Rapid Cloning of Amplified and Hypermethylated Human DNA Sequences from Restriction Landmark Genome Scanning Gels. Genomics, *58:* 254-262, 1999.
37. Dai, Z., Zhu, W. G., Morrison, C. D., Brena, R. M., Smiraglia, D. J., Raval, A., Wu, Y. Z., Rush, L. J., Ross, P., Molina, J. R., Otterson, G. A., and Plass, C. A comprehensive search for DNA amplification in lung cancer identifies inhibitors of apoptosis cIAP1 and cIAP2 as candidate oncogenes. Hum Mol Genet, *12:* 791-801, 2003.
38. Yu, L., Liu, C., Bennett, K., Wu, Y. Z., Dai, Z., Vandeusen, J., Opavsky, R., Raval, A., Trikha, P., Rodriguez, B., Becknell, B., Mao, C., Lee, S., Davuluri, R. V., Leone, G., Van den Veyver, I. B., Caligiuri, M. A., and Plass, C. A NotI-EcoRV promoter library for studies of genetic and epigenetic alterations in mouse models of human malignancies. Genomics, *84:* 647-660, 2004.
39. Zardo, G., Tiirikainen, M. I., Hong, C., Misra, A., Feuerstein, B. G., Volik, S., Collins, C. C., Lamborn, K. R., Bollen, A., Pinkel, D., Albertson, D. G., and Costello, J. F. Integrated genomic and epigenomic analyses pinpoint biallelic gene inactivation in tumors. Nat Genet, *32:* 453-458, 2002.
40. Smiraglia, D. J., Kazhiyur-Mannar, R., Oakes, C. C., Wu, Y. Z., Liang, P., Ansari, T., Su, J., Rush, L. J., Smith, L. T., Yu, L., Liu, C., Dai, Z., Chen, S. S., Wang, S. H., Costello, J., Ioshikhes, I., Dawson, D. W., Hong, J. S., Teitell, M. A., Szafranek, A., Camoriano, M., Song, F., Elliott, R., Held, W., Trasler, J. M., Plass, C., and Wenger, R. Restriction Landmark Genomic Scanning (RLGS) spot identification by second generation virtual RLGS in multiple genomes with multiple enzyme combinations. BMC Genomics, *8:* 446, 2007.
41. Ehrich, M., Nelson, M. R., Stanssens, P., Zabeau, M., Liloglou, T., Xinarianos, G., Cantor, C. R., Field, J. K., and van den Boom, D. Quantitative high-

throughput analysis of DNA methylation patterns by base-specific cleavage and mass spectrometry. Proc Natl Acad Sci U S A, *102:* 15785-15790, 2005.
42. Coolen, M. W., Statham, A. L., Gardiner-Garden, M., and Clark, S. J. Genomic profiling of CpG methylation and allelic specificity using quantitative high-throughput mass spectrometry: critical evaluation and improvements. Nucleic Acids Res, *35:* e119, 2007.
43. Costello, J. F., Fruhwald, M. C., Smiraglia, D. J., Rush, L. J., Robertson, G. P., Gao, X., Wright, F. A., Feramisco, J. D., Peltomaki, P., Lang, J. C., Schuller, D. E., Yu, L., Bloomfield, C. D., Caligiuri, M. A., Yates, A., Nishikawa, R., Su Huang, H., Petrelli, N. J., Zhang, X., O'Dorisio, M. S., Held, W. A., Cavenee, W. K., and Plass, C. Aberrant CpG-island methylation has non-random and tumour-type-specific patterns. Nat Genet, *24:* 132-138., 2000.
44. Smiraglia, D. J. and Plass, C. The study of aberrant methylation in cancer via restriction landmark genomic scanning. Oncogene, *21:* 5414-5426, 2002.
45. Shen, L., Guo, Y., Chen, X., Ahmed, S., and Issa, J. P. Optimizing annealing temperature overcomes bias in bisulfite PCR methylation analysis. Biotechniques, *42:* 48, 50, 52 passim, 2007.
46. Warnecke, P. M., Stirzaker, C., Melki, J. R., Millar, D. S., Paul, C. L., and Clark, S. J. Detection and measurement of PCR bias in quantitative methylation analysis of bisulphite-treated DNA. Nucleic Acids Res, *25:* 4422-4426., 1997.
47. Ushkaryov, Y. A. and Sudhof, T. C. Neurexin III alpha: extensive alternative splicing generates membrane-bound and soluble forms. Proc Natl Acad Sci U S A, *90:* 6410-6414, 1993.
48. Ushkaryov, Y. A., Petrenko, A. G., Geppert, M., and Sudhof, T. C. Neurexins: synaptic cell surface proteins related to the alpha-latrotoxin receptor and laminin. Science, *257:* 50-56, 1992.
49. Tabuchi, K. and Sudhof, T. C. Structure and evolution of neurexin genes: insight into the mechanism of alternative splicing. Genomics, *79:* 849-859, 2002.
50. Smiraglia, D. J., Smith, L. T., Lang, J. C., Rush, L. J., Dai, Z., Schuller, D. E., and Plass, C. Differential targets of CpG island hypermethylation in primary and metastatic head and neck squamous cell carcinoma (HNSCC). J Med Genet, *40:* 25-33, 2003.
51. Smith, L. T., Lin, M., Brena, R. M., Lang, J. C., Schuller, D. E., Otterson, G. A., Morrison, C. D., Smiraglia, D. J., and Plass, C. Epigenetic regulation of the tumor suppressor gene TCF21 on 6q23-q24 in lung and head and neck cancer. Proc Natl Acad Sci U S A, *103:* 982-987, 2006.
52. Hartwell, K. A., Muir, B., Reinhardt, F., Carpenter, A. E., Sgroi, D. C., and Weinberg, R. A. The Spemann organizer gene, Goosecoid, promotes tumor metastasis. Proc Natl Acad Sci U S A, *103:* 18969-18974, 2006.
53. Bonkhoff, H. Neuroendocrine differentiation in human prostate cancer. Morphogenesis, proliferation and androgen receptor status. Ann Oncol, *12 Suppl 2:* S141-144, 2001.
54. Nelson, E. C., Cambio, A. J., Yang, J. C., Ok, J. H., Lara, P. N., Jr., and Evans, C. P. Clinical implications of neuroendocrine differentiation in prostate cancer. Prostate Cancer Prostatic Dis, *10:* 6-14, 2007.

Acknowledgements

We thank Ms. Ellen Karasik of the Foster lab and the Mouse Tumor Models Resource at RPCI for excellent technical assistance.

Figure Legends

FIGURE 1. TRAMP sample grouping and histology. **A.** Age and weight of TRAMP samples. TRAMP sample groups and age and weight ranges are as follows: Prostatic Intraepithelial Neoplasia (PIN, 10-12 weeks, 0.008-0.04 gms), Well Differentiated (WD, 15-20 weeks, 0.03-0.09 gms), Early Poorly Differentiated Tumors (EPD, 15-20 weeks, 0.49-4.86 gms), and Late Poorly Differentiated Tumors (LPD, 22-28 weeks, 1.65-15-65 gms). Normal strain-matched prostates were uniformly small regardless of age. The sample key is shown on right. **B.** Representative H&E staining of each sample group.

FIGURE 2. Dnmt protein overexpression during TRAMP tumor progression. **A.** Representative Western blot images of Dnmt1, Dnmt3a, Dnmt3b, and Cyclin A in normal prostates (N) and TRAMP samples (PIN, WD, EPD, and LPD). The arrow on the Dnmt3a blot indicates the position of Dnmt3a (upper band), as determined by Western analysis of cell lines containing a genetic disruption of Dnmt3a (data not shown). Representative Ponceau S total protein staining is shown, and served as a loading control. Densitometric quantification of Dnmt1 **(B)**, Dnmt3a **(C)**, Dnmt3b **(D),** and Cyclin A **(E)** Western blots, showing all analyzed samples. Dots represent individual samples and horizontal bars indicate the mean of each sample group. Dnmt1 **(F),** Dnmt3a **(G),** and Dnmt3b **(H)** protein expression normalized by Cyclin A. Mann-Whitney test p-values: ** $p < 0.005$; * $p < 0.01$, for each group compared to normal prostate.

FIGURE 3. Locus-specific DNA hypermethylation during TRAMP tumor progression. **A.** RLGS analysis showing Spot 3C21, corresponding to *Nrnx2* (solid circle). The dashed circle illustrates the position of spot loss (hypermethylation event), seen exclusively in the EPD and LPD samples. **B.** RLGS analysis showing Spots 3D22 (upper spot) and 3E30 (lower spot), corresponding to *Cdkn2a* and *Gsc*, respectively (solid circles). The dashed circles illustrate the position of spot loss (hypermethylation events), seen exclusively in the EPD and LPD samples. **C.** RLGS spot losses (hypermethylation events) and RLGS spot gains (hypomethylation events) in each sample group. Error bars indicate +/- 1 SD. **D.** Hypermethylation events in each sample analyzed by RLGS. Dots represent individual samples and horizontal bars indicate the mean of each sample group.

FIGURE 4. Downstream hypermethylation and increased expression of Cdkn2a genes during TRAMP tumor progression. Expression of *p19ARF* **(A)** and *p16INK4a* **(B)** in normal prostates and TRAMP tumor samples. mRNA copy number is normalized relative to *18s rRNA* copy number. Dots represent individual samples and horizontal bars indicate the mean of each sample group. Mann-Whitney test p-values: ** $p < 0.006$; * $p < 0.05$, for each group compared to normal prostate. **C.** Top: diagram of the Cdkn2a locus. Open rectangles, p19 exons; hashed rectangles, p16 exons; lines, introns; right

arrows, transcriptional start sites; vertical arrow, position of the NotI site identified by RLGS; black rectangles, CpG islands; horizontal line with circles (A-C), regions analyzed by sodium bisulfite sequencing. Bottom: sodium bisulfite sequencing data of regions A-C in normal prostate and TRAMP samples. Percent methylation (averaged over the entire sequenced region), from at least ten sequenced clones per sample, is plotted. Asterisks are shown above samples that displayed ≤ 1 % methylation.

FIGURE 5. Downstream hypermethylation and increased expression of Cacna1a during TRAMP tumor progression. **A.** Expression of *Cacna1a* in normal prostates and TRAMP tumor samples. mRNA copy number is normalized relative to *18s rRNA*. Dots represent individual samples and horizontal bars indicate the mean of each sample group. Mann-Whitney test p-value: ** $p < 0.006$, for each group compared to normal prostate. **B.** Top: diagram of the Cacna1a locus. Right arrow, transcriptional start site; open rectangles, exons; lines, introns; vertical arrow, position of the NotI site identified by RLGS; black bar, CpG island; horizontal line with circles (A and B), regions analyzed by sodium bisulfite sequencing. Bottom: sodium bisulfite sequencing data of regions A and B in normal prostate and TRAMP samples. Percent methylation (averaged over the sequenced entire region), from at least ten sequenced clones per sample, is plotted. Asterisks are shown above samples that displayed ≤ 1 % methylation.

FIGURE 6. DNA hypomethylation during TRAMP tumor progression. **A.** 5mdC levels in normal prostates and TRAMP samples. 5mdC levels were determined by LC-MS as described in the *Materials and Methods*. Sample groups are the same as described in Fig. 1A. Dots represent individual samples and horizontal bars indicate the mean of each sample group. Mann-Whitney test p-values: ** $p < 0.005$; * $p < 0.05$, for each group compared to normal prostate. **B.** B1 methylation in normal prostates and TRAMP samples. Methylation of the mouse B1 repetitive element was determined by quantitative bisulfite pyrosequencing as described in the *Materials and Methods*. Dots represent individual samples and horizontal bars indicate the mean of each sample group. Mann-Whitney test p-values: ** $p < 0.005$; * $p < 0.05$, for each group compared to normal prostate. Correlation analysis of RLGS hypermethylation events and global 5mdC levels **(C)** or B1 repetitive element methylation **(D)** in TRAMP. Spearman Rank Order Correlation coefficients (r values) and p-values are shown.

FIGURE 7. DNA methylation pathway alterations during prostate cancer progression in TRAMP. The timing and relative extent of distinct alterations in the DNA methylation pathway are shown. The dashed line indicates a putative regulatory loop leading to increased Dnmt1 and Dnmt3b protein expression. Details of the model are explained in the *Discussion*.

Fig 1 Morey Kinney et al.

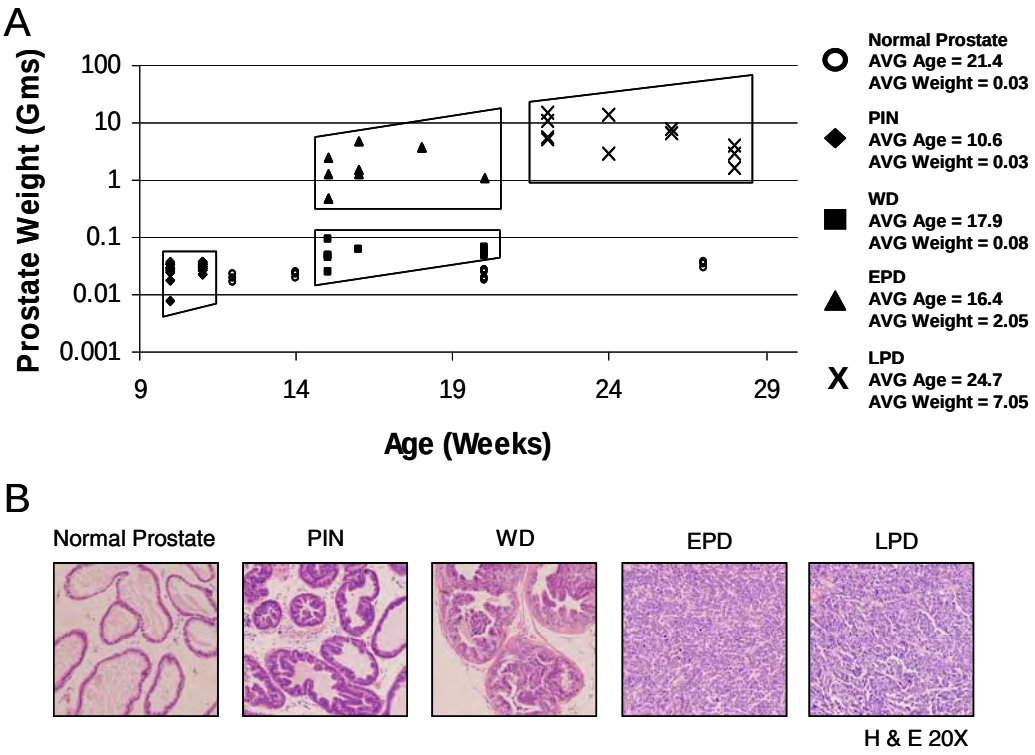

Figure 2. Morey Kinney et al.

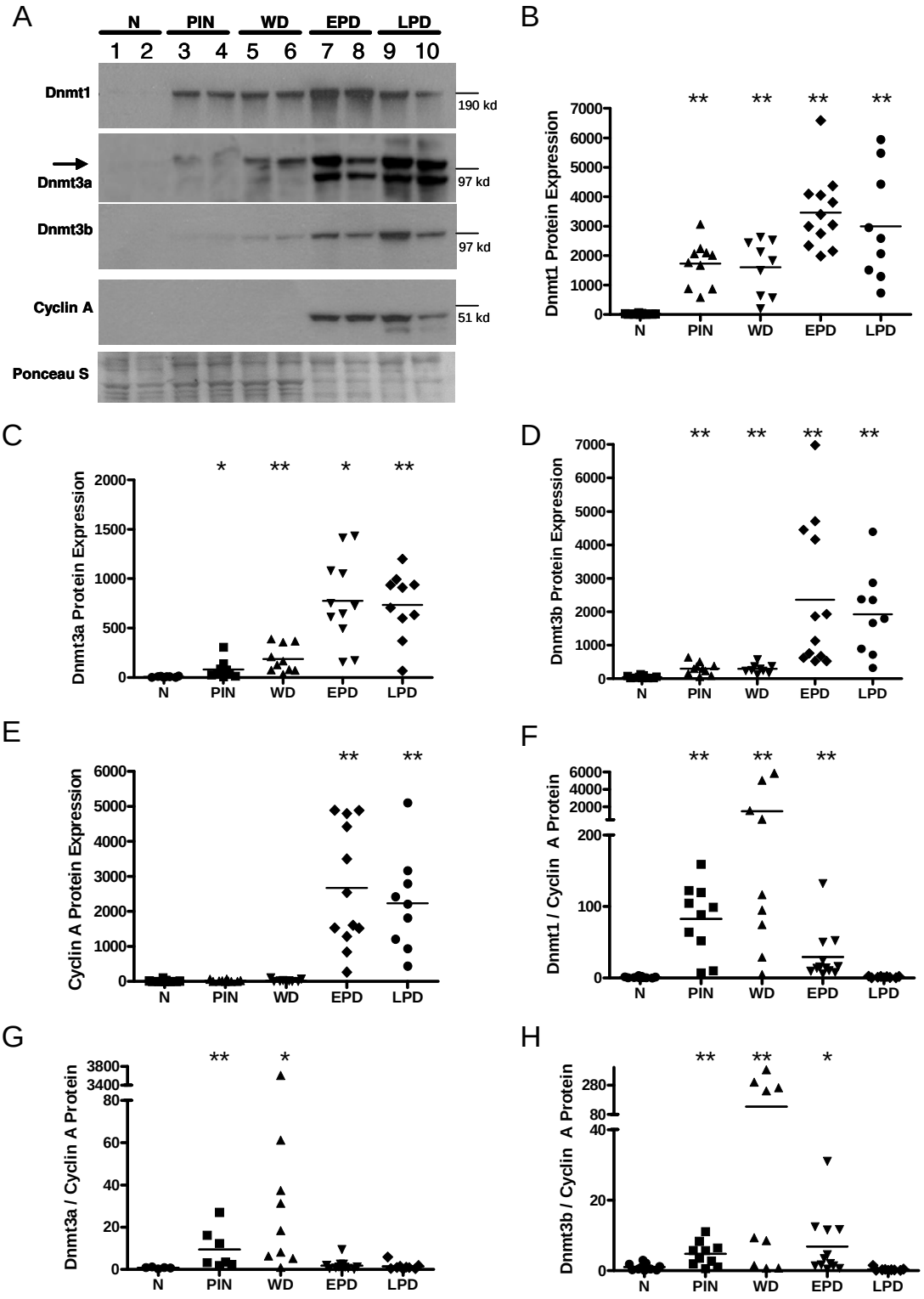

Figure 3. Morey Kinney et al.

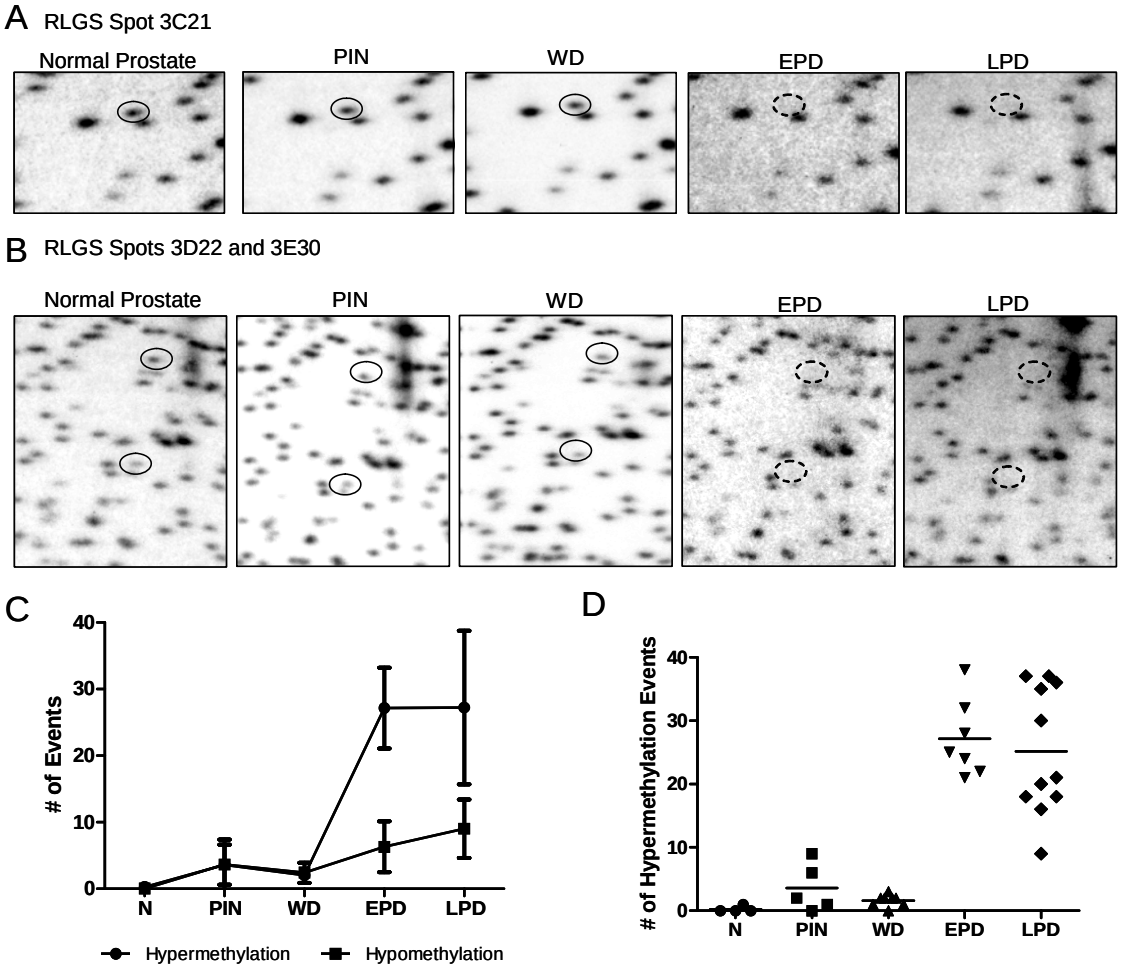

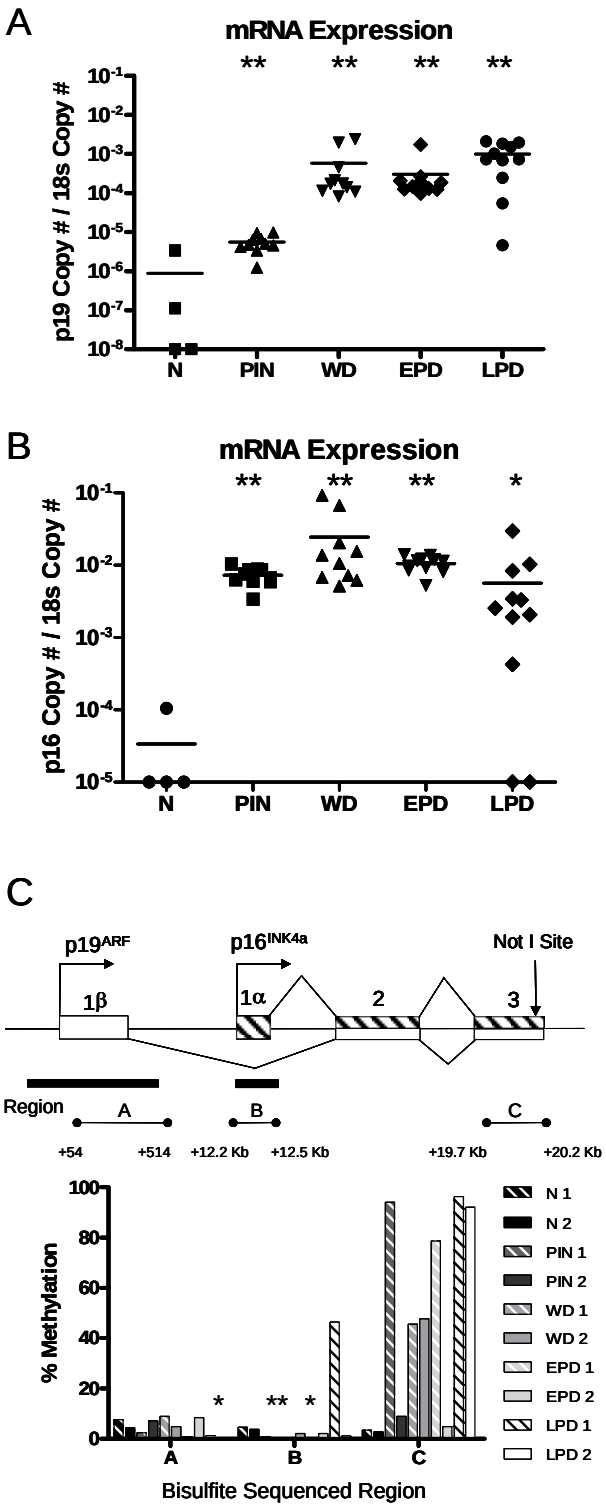

Fig 4.

Morey Kinney et al.

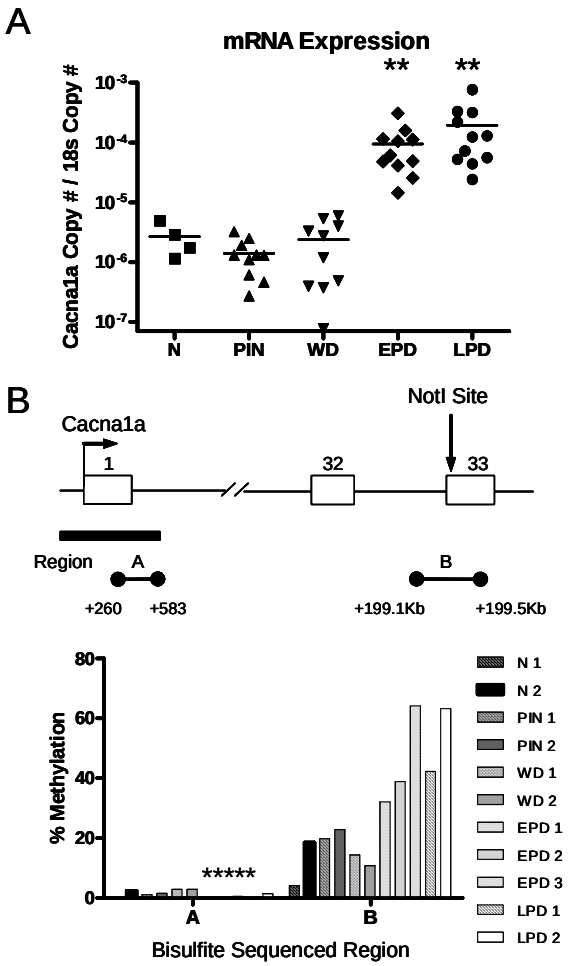

Fig 5.

Morey Kinney et al.

Fig 6. Morey Kinney et al.

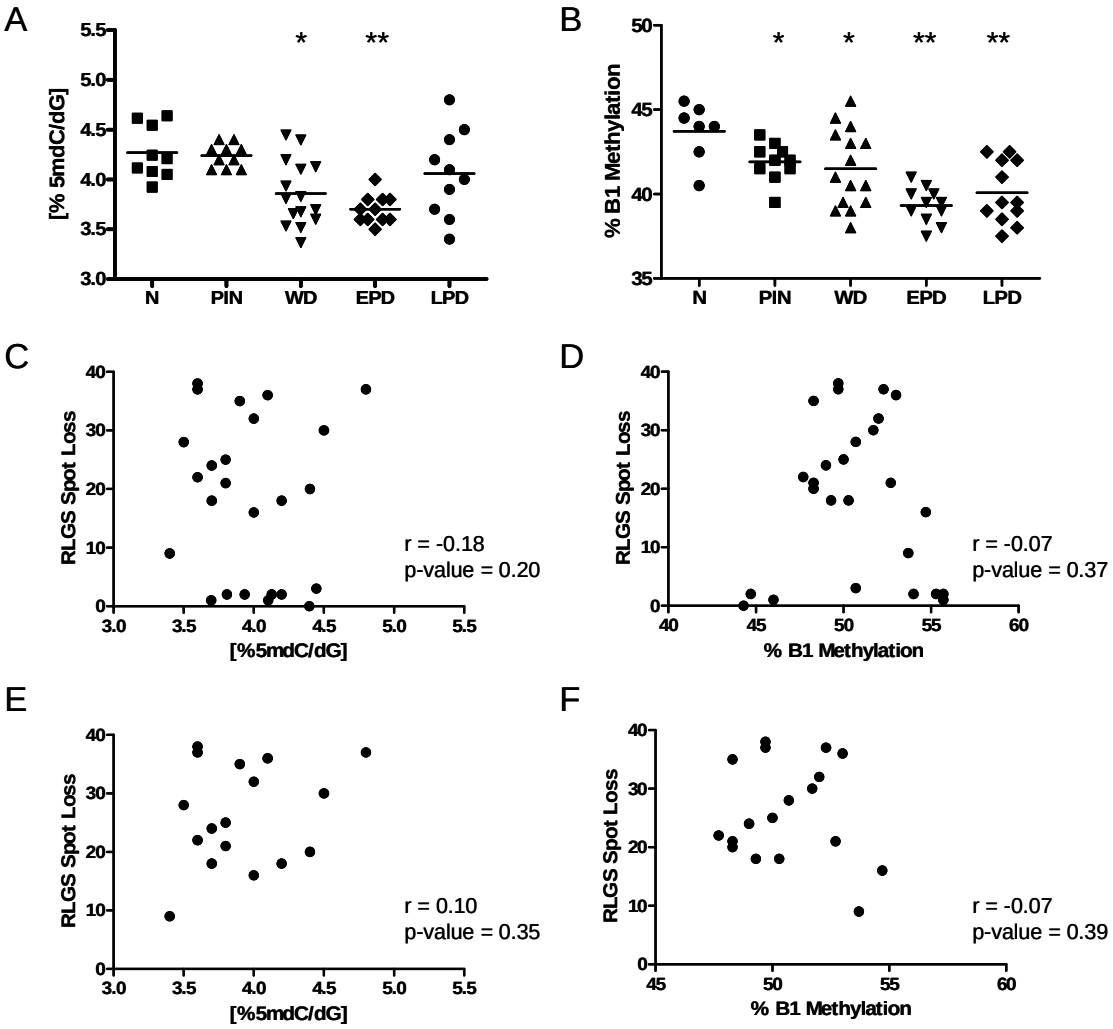

Fig. 7. Morey Kinney et al.

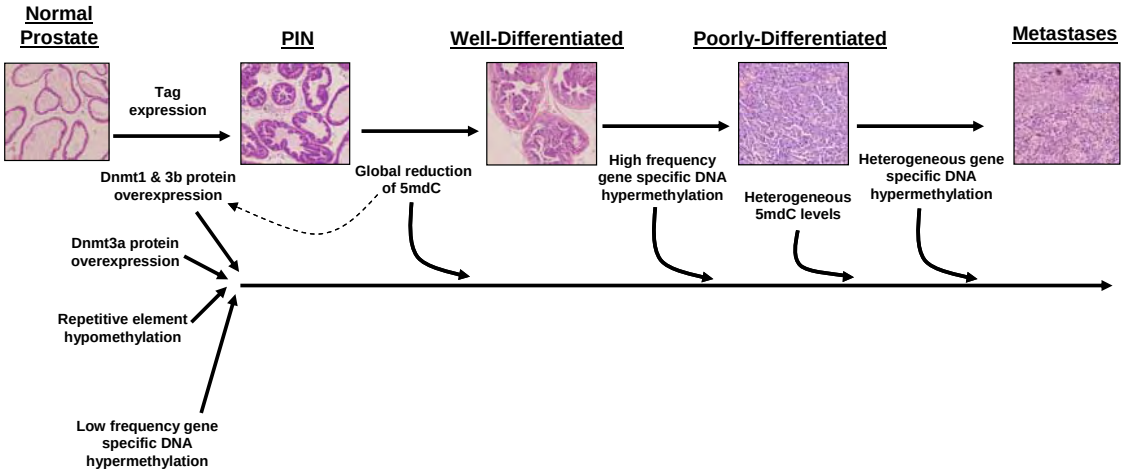

Publication 2

Phenotype-specific CpG Island Methylation Events in a Murine Model of Prostate Cancer.

Cancer Research. 2008. (In press)

Marta Camoriano[1]*, Shannon R Morey Kinney[2]*, Michael T Moser[2], Barbara A Foster[2], James L Mohler[3], Donald L Trump[3], Adam R Karpf[2], Dominic J Smiraglia[1,†]

Departments of [1]Cancer Genetics, [2]Molecular Pharmacology and Cancer Therapeutics, and [3]Urologic Oncology, Roswell Park Cancer Institute, Buffalo, NY, USA, 14263

*These authors contributed equally to this work

[†]***Corresponding author:***

Dominic J Smiraglia, PhD
Department of Cancer Genetics
Roswell Park Cancer Institute
Buffalo Life Science Complex, Rm. L3-314
Buffalo Niagara Medical Campus
Elm + Carlton Streets
Buffalo, NY 14263
Email: Dominic.Smiraglia@roswellpark.org
Phone: (716) - 845 - 1347
Fax: (716) - 845 – 1698

Running title:
CpG island Methylation in TRAMP Model

Abstract
Aberrant DNA methylation plays a significant role in nearly all human cancers, and may contribute to disease progression to advanced phenotypes. Study of advanced prostate cancer phenotypes in the human disease is hampered by limited availability of tissues. We therefore took advantage of the Transgenic Adenocarcinoma of Mouse Prostate (TRAMP) model to study whether three different phenotypes of TRAMP tumors (PRIM - late stage primary tumors, AIP - androgen-independent primary tumors, and MET - metastases) displayed specific patterns of CpG island hypermethylation using Restriction Landmark Genomic Scanning (RLGS). Each tumor phenotype displayed numerous hypermethylation events, with the most homogeneous methylation pattern in AIP and the most heterogeneous pattern in MET. Several loci displayed a phenotype-specific methylation pattern; the most striking pattern being loci methylated at high frequency in PRIM and AIP, but rarely in MET. Examination of the mRNA expression of three genes, BC058385, Goosecoid, and Neurexin 2, which exhibited non-promoter methylation, revealed increased expression associated with downstream methylation. Only methylated

samples showed mRNA expression, in which tumor phenotype was a key factor determining the level of expression. The CpG island in the human ortholog of BC058385 was methylated in human AIP, but not in primary androgen-stimulated prostate cancer or benign prostate. The clinical data demonstrate a proof-of-principle that the TRAMP model can be used to identify targets of aberrant CpG island methylation relevant to human disease. In conclusion, phenotype-specific hypermethylation events were associated with the over expression of different genes and may provide new markers of prostate tumorigenesis.

Introduction

Prostate cancer (CaP) is the most commonly diagnosed cancer in American men (12). Molecular markers, such as prostate-specific antigen (PSA), have increased chances of diagnosing CaP at its earliest stages (12). Treatment options for primary prostate cancer (PRIM) detected early include radical prostatectomy, radiation therapy, and active surveillance (12). At the time of diagnosis, approximately 30% of men have disease that extends beyond the prostate gland- some have clinically metastatic (MET) disease at the time of diagnosis and others suffer clinical or biochemical recurrence after potentially curative radical prostatectomy or radiation therapy. Advanced CaP is usually treated by testicular androgen deprivation therapy (ADT) using surgical or medical castration (12). However, for most men, CaP will recur in this androgen-depleted environment as a disease commonly referred to as androgen-independent CaP (AIP) (13, 14). There are currently no dependable biomarkers to determine which cancers will be most likely to be highly aggressive and eventually develop into AIP and/or MET disease.

DNA methylation is an epigenetic modification of the DNA that is frequently disrupted in nearly all types of cancer. Hypomethylation of repetitive elements is frequently seen and hypermethylation of specific CpG islands in promoter regions of several tumor suppressor genes are commonly observed to be associated with the transcriptional silencing of the gene (15-19). Although less well studied, methylation of non-promoter CpG islands in the 3' ends or bodies of genes has been associated with ectopic, or over expression of genes such as *PAX6* (20, 21), *p16* (2) and others (22).

In recent years, DNA methylation has been touted as an ideal target for the development of cancer biomarkers (19, 23, 24). The most common CpG island methylated in CaP is the *GSTP1* gene, for which some reports have demonstrated methylation in >90% of primary CaP (25, 26). However, studies focusing specifically on the molecular biology of androgen-independent and/or metastatic CaP directly in human tissues rather than cell lines are limited. A major reason for this is the difficulty in obtaining these tissues. Given improved screening using digital rectal examination and PSA testing, most men present with indications for the disease prior to clinically evident metastatic spread. Those patients that present with metastatic disease are treated by ADT rather than surgery. Recurrence during ADT is not generally treated surgically as the recurrence typically occurs at multiple metastatic sites. Even rarer is the collection of metastatic tumors from patients who have not received ADT. However, since the metastatic phenotype can be acquired prior to ADT, a cell's metastatic potential and its ability to grow independent of androgen stimulation are separable phenotypes. Therefore, different molecular events may underlie the acquisition of these two phenotypes. The rarity of these tissues available for research and the difficulty in

separating the metastatic and androgen-independent phenotypes has limited investigation into the molecular basis of these phenotypes at the genomic level.

To circumvent some of these difficulties, human CaP cell lines have been used extensively to study the molecular biology of CaP. These cell line models have led to a number of important observations that have been confirmed in human tumor tissues (27, 28). However, we have demonstrated that cell lines provide exceptionally poor models for genomic screening to identify CpG island hypermethylation events (29). Recently, several studies have been completed using the TRansgenic Adenocarcinoma of Mouse Prostate (TRAMP) model in which disruption of the DNA methylation pathway was observed. Dnmts were found to be over expressed in late stage TRAMP primary tumors and metastases to liver, kidney and lymph node. Furthermore, non-random hypermethylation of CpG islands in late stage TRAMP primary tumors was also reported (2).

The TRAMP model utilizes the rat probasin promoter to drive expression of SV40 early genes (large and small T antigens) in prostatic epithelium (30). Oncogene expression leads to further genetic and/or epigenetic changes that result in prostate tumor formation and disease progression to metastases at several sites in the mouse (31). Castration of TRAMP mice leads to tumor regression and increased survival (32, 33). However, some of the mice develop androgen-independent primary tumors that often are more aggressive and also metastasize (32, 33).

In the current study, the TRAMP model system was used to study CpG island hypermethylation in CaP in three tumor phenotypes – primary (PRIM), metastatic (MET), and androgen-independent (AIP) – to determine if DNA methylation differences existed among them. Numerous high frequency methylation events and phenotype-specific events were identified, which included three genes whose expression was increased in methylated samples dependent upon tumor phenotype.

Materials and Methods

Animals and tissue samples.

Restriction Landmark Genomic Scanning (RLGS) was performed on 4 benign prostate DNAs from nontransgenic mice and a total of 90 TRAMP tumors. All tumors came from TRAMP mouse F_1 generation males from the cross TRAMP X FVB, with the TRAMP mothers on a C57BL/6 background. All androgen-dependent primary prostate tumors (PRIM) and metastases (MET) were collected from different mice without androgen deprivation. For the intraprostatic androgen-independent tumors (AIP), animals were castrated at 12 weeks of age (after primary tumor formation had begun) and recurring tumors were collected 12 weeks later. A total of 30 PRIM, 30 MET (from liver and lung), and 30 AIP tumors were analyzed.

Human Tissues

The androgen-stimulated benign prostate (AS-BP) samples were obtained from patients treated for lower urinary tract symptoms by transurethral prostatectomy. The androgen-stimulated primary prostate cancer (AS-CaP) samples were obtained from patients treated for CaP by prostatectomy. The recurrent primary tumors (RCaP) were obtained by transurethral resection from patients who presented with urinary retention from recurrent CaP during ADT (34). AS-CaP and AS-BP were enriched to > 70% epithelial cells using standard microdissection of 20 μm frozen step sections adjacent to 8

μm sections identified by H&E staining to contain more than 50% epithelial cells, as previously described (35). RCaP did not require microdissection as it was composed of an average of 92% malignant cells (34).

Restriction landmark genomic scanning and spot cloning

The protocol for extraction of genomic DNA from tissues was described previously (36). The published protocol of Dai et al. (2003) (37) was followed for RLGS gels. RLGS spots of interest were cloned as previously described (36, 38-40) .

Quantitative Real Time RT-PCR (qRT-PCR)

RNA samples were extracted from mouse tissues using Trizol reagent (Invitrogen) and converted to cDNA using random hexamer and oligo-dt primers by 'First strand cDNA synthesis kit' (Fermentas). PCR reactions were conducted using the qPCR MasterMix Plus for SYBR Green I (Eurogentec, San Diego, CA) Primer sets, shown in Supplemental Table 1, for specific amplification were obtained from IDT. Absolute quantification was used to determine gene expression copy number normalized to 18S rRNA. All reactions were performed in triplicate and the data are presented as the mean 18S normalized quantity X 10,000.

Sodium Bisulfite Treatment

Sodium bisulfite treatment to convert unmethylated cytosine to thymidine was completed following the manufacturer's protocol EZ-96 DNA Methylation Kit (Zymo Research, Orange, CA) using 750 ng in 50 μl of distilled water and M-Dilution Buffer. The treated samples were resuspended in 75 μl of M-Elution Buffer and stored at -20°C.

MassARRAY Quantitative Methylation Analysis (MAQMA)

MassArray Quantitative Methylation Analysis (MAQMA) was performed using the MassARRAY Compact system developed by the Sequenome Company, as previously described (41), using the primers shown in Supplemental Table 2. This system utilizes mass spectrometry (MS) for the detection and quantitative analysis of DNA methylation. This approach has been shown to a be highly accurate and reproducible way to quantitate methylation (42) Regions near the RLGS spots of interest to be analyzed were determined as follows: For spots 2G63 and 3C21, which were within CpG islands, we sequenced a region within the islands. For spot 5F09, which was not within a CpG island, nor near the 5' end of the gene, we sequenced a region encompassing the NotI site.

Statistics

All statistical analyses were performed using the Graph Pad Prism 5 software. To test for normality of distribution of data, D'Agostino & Pearson omnibus normality test was used. To test for differences between two groups with non-normal distribution, a student's t-test with Welch's correction factor was used. To test for differences among more than two groups with non-normal distribution, the Kruskal-Wallis test was used. To test for correlation between methylation % and expression levels, the Spearman's Rank Order correlation test was used.

Results

Genomic scanning of CpG island methylation in TRAMP tumors

To identify CpG island hypermethylation in CaP from the TRAMP model, we performed restriction landmark genomic scanning (RLGS). RLGS profiles of benign prostatic DNA collected from four different animals from the cross C57BL/6 X FVB $_{F1}$ produced the same pattern of RLGS spots. A region of the profile containing 1445 spots was found to be resolvable in all tumor gels and was analyzed in all 90 TRAMP tumor RLGS profiles compared to a single benign prostate tissue DNA RLGS profile. Any spot absent or greatly reduced in intensity in the tumor profile was considered lost, and therefore methylated as, previously demonstrated (2, 43, 44). The numbers of RLGS spots lost for each of the three groups of 30 tumors studied is shown in Supplemental Table 3 and analyzed in Figure 1. An average of 32, 36, and 31 RLGS spots were lost (hypermethylation events) in PRIM, AIP, and MET tumors, respectively (Table S3 and Fig 1A). Although there was no significant difference in the average number of methylated loci in each group, there was significantly more variability among samples in the MET group compared to either the PRIM or AIP groups. The PRIM and AIP groups showed nearly identical distributions of the total number of methylated loci in each of the 30 samples, whereas the MET group exhibited a significantly different distribution with some samples having greater than 80 methylated loci and others with as few as 12 (Table S3, Fig 1A).

Despite the fact that the distribution of total numbers of methylated loci was nearly identical between PRIM and AIP, the frequency at which specific loci were methylated within the groups differed (Fig 1B). Although the number of loci methylated in any sample was lowest in the AIP group, these loci were methylated at a higher frequency within the AIP group than either the PRIM or MET groups (Fig 1B). Comparing the three phenotypes, the AIP group displayed the highest percentage of RLGS spots that were methylated in 26-30 of the samples (Fig 1B), whereas the MET group had the largest proportion of loci methylated in only 6-10 samples. These data indicate that the AIP tumors have the most homogeneous pattern of RLGS spot methylation, while the MET group has the most heterogeneous.

Totals of 222, 212, and 270 RLGS spots were methylated at least once in the PRIM, AIP, and MET groups of samples, respectively. Limiting the analysis to spots methylated minimally 3 times out of 30 within each phenotype, 89, 93 and 106 such spots, respectively, were found. A total of 48 loci were hypermethylated at least once in all three phenotypes (Fig 1C). The number of spots lost in two of the three phenotypes decreased to 10, 10, and 15 for the combinations of PRIM+MET, AIP+MET, and PRIM+AIP, respectively (Fig 1C). These data indicate that the two primary tumor phenotypes are more similar to each other than they each are to the metastatic phenotype. In addition, the number of loci hypermethylated in a single phenotype (PRIM = 16, AIP = 20, and MET = 38) suggests more heterogeneity in the MET samples compared to the PRIM samples (Fig 1C).

Tumor phenotype-specific hypermethylation of RLGS spots

Table 1 shows the RLGS spots of interest based on their pattern of loss among the three phenotypes. A total of 13 RLGS spots were lost in greater than 33% of the samples regardless of phenotype. The most frequently lost spot was 3D22, which was lost in 82 of the 90 samples. This RLGS spot has been identified in the 3' end of the Cdkn2a locus.

We have previously demonstrated that the promoter region of p19 and p16 were not methylated in TRAMP tumors and the 3' end methylation detected by RLGS was associated with over expression (2).

Although no RLGS spot losses were specific to either the PRIM or MET phenotypes, six loci showed significant specificity for the AIP phenotype. More striking was the observation that 13 loci showed a significant association of methylation with the PRIM and AIP phenotypes, but little or no methylation in the MET tumors (Table 1). The strongest example of which was spot 3C21 (spot # 1, Table 1), lost in 20 PRIM and 27 AIP tumors, but only 1 MET lesion. Supplemental Figure 1 shows representative examples of RLGS gel analysis with 4C38 (spot # 23, Table 1) representing a locus lost at high frequency regardless of phenotype (Fig S1A), spots 3C21 and 2G63 (spot # 1, Table 1) lost only in PRIM and AIP (Fig S1B, C), and spot 4D69 (spot # 4, Table 1) lost exclusively in AIP samples (Fig S1D). These observations support the hypothesis that different tumor phenotypes display a specific methylation pattern.

Mass Array Quantitative Methylation Analysis of RLGS loci of interest

RLGS spot loss is based on the methylation of critical CpGs in the target sequence of the NotI enzyme. In order to confirm the specificity of methylation to the PRIM and AIP phenotypes observed by RLGS, and further, to determine if methylation of the NotI site indicated methylation in the surrounding region, three of the four RLGS loci that showed the strongest prevalence for methylation in the PRIM or AIP phenotypes were analyzed using Mass Array Quantitative Methylation Analysis (MAQMA) on all 90 tumor samples. MAQMA gives a quantitative value of percent methylation at each informative CpG dinucleotide. A diagrammatic representation of the data for half the samples in each phenotype for 2G63 and 3C21 is shown in Supplemental Figure 2. The MAQMA analysis confirmed the phenotype-specificity identified by RLGS demonstrating methylation of these loci specifically in PRIM and AIP tumors, but not MET tumors.

In order to get a single value for comparison purposes between RLGS and MAQMA data, the average percent methylation of all the CpG dinucleotide in each of the 90 samples was plotted in Figure 2. Methylation of the NotI site by RLGS analysis matched quite well with methylation of the surrounding DNA for spots 2G63 and 5F09 (spot # 3, Table 1). Only a small number of cases exhibited discordance between the two approaches (Fig S2A and Fig 2A, C). This was particularly clear for 2G63 (Fig 2A); the only AIP tumor of 30 that did not show RLGS spot loss also showed very low methylation by MAQMA. However, for spot 3C21, we observed that several of the samples expected to be methylated based on RLGS analysis had less than 50% methylation (Fig S2B and Fig 2B). Nevertheless, all samples that were unmethylated as shown by RLGS displayed very low levels of methylation by MAQMA.

This and all bisulfite sequencing based approaches can underestimate methylation due to PCR bias against the methylated alleles. The potential for such PCR bias has been documented by multiple groups and shown to be very amplicon dependent (45, 46). To assess the possibility of bias against amplification of methylated alleles we *in vitro* methylated (IVM) an aliquot of commercially available peripheral blood lymphocyte (PBL) DNA with SssI methylase, which methylates all CpG dinucleotides. Various ratio mixtures of the normal DNA with the IVM DNA were prepared, creating 100%, 75%, 50%, 25%, and 0% IVM DNA controls. These control DNAs were bisulfite treated and

used as template for bisulfite PCR and MAQMA analysis. Examination of the control samples for each of the MAQMA primer sets revealed that, while 2G63 and 5F09 had very little bias, 3C21 displayed a strong bias toward unmethylated product, particularly between 25% and 75% expected methylation (Fig S2A, B and Fig 2D). This bias resulted in a lower observed percent methylation than expected for 3C21 (Fig 2D). These data indicate that RLGS analysis is a good predictor of methylation within an entire region surrounding the NotI site.

Expression of phenotype-specific hypermethylated genes in TRAMP

DNA methylation is an important mechanism for regulating gene transcription and has been most commonly associated with gene silencing when found at the 5' ends of genes. Most RLGS loci hypermethylated in cancer come from CpG islands in the 5' ends of genes. However, for the set of eight genes that were specifically methylated in PRIM and AIP, but not MET, >60% were found in the body or 3' end of the gene (Table 1). We chose three such RLGS loci (2G63, 3E30, and 3C21) to study the relationship between body of the gene or 3' end methylation and expression.

Using quantitative reverse transcription PCR (qRT-PCR), the mRNA expression of the 2G63 transcript, BC058385, where the methylated CpG island surrounds the fourth exon, was measured in Figure 3. Increased expression correlated with increased methylation (Fig 3B) (Spearman's Rank Order Correlation $r=0.756$; $p<0.0001$) using RNA from 15 samples in each phenotype (samples were chosen to include both methylated and unmethylated examples in each phenotype). No expression and very little methylation were observed in normal prostate. Though methylation of this locus was primarily seen in PRIM and AIP tumors, there were eight MET tumors with methylation. We analyzed expression in six and found that all six showed little or no expression. This is in contrast to the methylated PRIM and AIP samples, approximately half of which showed expression when methylated (Fig 3B). These results indicate a separate mechanism in conjunction with DNA methylation that may be regulating expression of these genes in a phenotype-specific manner.

Expression of the Goosecoid (*Gsc*) homeobox gene (3E30 -spot # 2, Table 1) was also measured using qRT-PCR. This locus is unique in that the NotI site is not contained within a CpG island but is within the third exon at the 3' end of the gene approximately 2kb away from the CpG island encompassing the transcriptional start site (Fig 3). MAQMA analysis surrounding the transcriptional start site showed no methylation (data not shown) in any of the 90 samples despite methylation of the 3' NotI site in 24 PRIM, 29 AIP, and 5 MET samples. Quantitative expression analysis demonstrated that none of the unmethylated samples showed expression of *Gsc*, but some of the methylated samples did (Fig 3C). Furthermore, after separating the data by phenotype, it became clear that the few MET samples that had methylation of the 3' NotI site also had the highest levels of expression as a group (Fig 3D).

DNA methylation and expression from the Neurexin 2 α and β promoters

The most striking example of phenotype-specificity of CpG island methylation was RLGS spot 3C21, which was lost in 20/30 PRIM, 27/30 AIP, and only 1/30 MET tumors (*p=1.0E-12* for specificity to PRIM and AIP). 3C21 represents a CpG island in exon 2 of the *Nrxn2* locus. There are two promoters for *Nrxn2* (α and β), which is a signature feature of the Neurexin family of genes (47-49), and each promoter is within a CpG island, as shown in Figure 4 (CpG islands A and C). The transcript from the β

promoter contains a unique first exon, but otherwise shares the same exons as the transcript from the α promoter from exon 17 onward (49). The NotI site analyzed by RLGS is found within CpG island B, located 9 kb downstream of the α promoter of *Nrxn2*. MAQMA analysis of all three CpG islands showed that the methylation at island B in exon 2 closely matched the methylation observed by RLGS; most of the PRIM and AIP tumors displayed robust hypermethylation (Fig 2B). However, little or no methylation was observed at either the α or the β promoter (CpG islands A and C) in any of the 90 samples (data not shown).

Using qRT-PCR and primers that were specific to each transcript (Fig 4), mRNA expression originating at both promoters was measured (Fig 4). We observed a significant increase in expression at the α promoter (Fig 4A) when CpG island B was hypermethylated 9 kb downstream. Furthermore, consistent with the methylation pattern, the over expression was only observed in the primary tumors and androgen-independent tumors, not in the metastases (Fig 4B). Expression for the β isoform of Nrxn2 did not correlate either positively or negatively with methylation at CpG island B. (Fig 4C, D). No correlation could be detected between usages of the α or β promoters (data not shown).

Aberrant methylation in TRAMP model conserved in human prostate cancer

In order to determine if novel targets of aberrant CpG island hypermethylation identified in the TRAMP model were relevant to the human disease, the methylation of the human orthologs of two RLGS loci were studied in sets of 13 human androgen-stimulated benign prostate (AS-BP), 13 androgen-stimulated primary prostate cancer (AS-CaP), and 12 primary tumor recurrences during androgen deprivation therapy (RCaP). MAQMA analysis was performed on the human samples for the orthologous regions in the human genome for the mouse RLGS spots 3C21 and 2G63. For spot 3C21, the human NRXN2 locus has the same structure as the mouse. However, we found no methylation in any of the human samples for CpG island B (data not shown). For spot 2G63, the orthologous region in the human genome matches a CpG island in the fourth exon of gene BC029292 on chromosome 7q11.23. The MAQMA data in the human samples, as shown in Figure 5, demonstrated little or no methylation in the AS-BP and AS-CaP (Fig 5A, B) samples but greater than 50% methylation was observed in 5/12 RCaP samples (Fig 5B, D). These data demonstrate a proof-of-principle that the loci identified as novel targets of methylation in the TRAMP model (Table 1) may be relevant to the human disease.

Discussion

These studies demonstrated that three different tumor phenotypes – PRIM, AIP, and MET - from the TRAMP model exhibited many hypermethylation events throughout the genome as well as phenotype-specific patterns of hypermethylation. Furthermore, the TRAMP model was used to identify CpG island methylation relevant to human CaP. Similar to previous studies (43, 50, 51), we found that methylation at the NotI site as measured by RLGS is a good indicator of the methylation in the surrounding region. Our findings led to the identification of gene over expression coinciding with downstream hypermethylation, which may or may not be contained within a CpG island. This is similar to previous findings of methylation of non-promoter CpG islands in the 3' ends or bodies of genes associated with ectopic, or over expression of genes such as *PAX6* (20,

21), *p16* (2) *PDX1* and *OTX1* (22). We showed that the BC058385 (RLGS spot 2G63) and Nrxn2 (RLGS spot 3C21) transcripts are over expressed when their downstream CpG islands are hypermethylated. We also found that *Gsc* expression is increased with hypermethylation of a downstream region that does not contain a CpG island, while the upstream CpG island showed no methylation in any samples.

It is striking that for *Gsc*, three of the five data points above the median level of expression in the methylated samples (Fig. 3D) come from the MET group, yet this is exactly the group showing the least number of cases with methylation. This is in contrast to the data from *Nrxn2* and the 2G63 transcript (Fig 3B and 4B), where only methylated samples showed expression but the MET samples showed no expression even in the few cases where the MET samples were methylated. These data suggest that methylation of the 3' ends of these genes is necessary, but not sufficient for their expression since none of the unmethylated samples show any expression, but a number of methylated samples also have no expression. In all three cases, however, tumor phenotype is the key to determining which of the methylated samples show expression. It does not seem likely that the 3' end methylation is driving the over expression given the large number of cases where methylation is seen without over expression. However, it may be the case that the 3' end methylation is a stabilizing factor in initiating transcription when other conditions are favorable for transcription of the gene. Nevertheless, what is clear is that only those cases with high level methylation at the 3' end of *Gsc* and the body of *Nrxn2* and the 2G63 transcript showed over expression in our data set and tumor phenotype was a strong factor in determining which methylated samples had over expression.

Gsc is a highly conserved transcription factor that is the most abundantly expressed homeobox gene in the Spemann organizer in *X. laevis* (52). Expression of this gene allows these cells go through epithelial to mesenchymal transition (EMT) during gastrulation and ingress into the interior of the embryo. It was recently demonstrated that ectopic expression of *GSC* is found in human breast tumors and this expression was shown to be able to induce EMT and increase the ability of cells to form metastases (52). We found that 53/60 TRAMP tumors at the primary site showed methylation in the 3' end of Gsc, yet most showed no expression. The MET tumors, however, showed methylation in only 5/30, but four of these five showed elevated *Gsc* expression, ranging from slightly to highly over expressed. We propose that the high rate of methylation we see in tumors at the primary site is a requisite early step in overcoming the negative regulation of *Gsc* put in place after embryogenesis, but not sufficient for ectopic expression. Those primary tumor cells that do acquire ectopic expression may have better ability to undergo EMT and acquire migration and survival abilities increasing their metastatic potential. In the metastatic tumors that develop, continued expression of *Gsc* may not be required, and the negative regulation of this gene may become re-established as reflected by the fact that most MET tumors do not exhibit methylation of the 3' end. In the few metastatic tumors where we observed 3' end methylation and varied levels of ectopic expression, perhaps the negative regulation of *Gsc* was not yet re-established.

Neurexin 2 has two promoters (α and β); both with CpG islands, plus a third CpG island in exon 2 located 9 kb downstream of the α promoter. We found that transcripts originating from the α promoter were over expressed when the internal CpG island was

hypermethylated. Both the α and β promoters were unmethylated in all 90 samples. Methylation of the internal CpG island does not appear to alter which of the two promoters is used. We could find no correlation between the level of α transcript and β transcript in each sample. Expression of the Nrxn family of proteins is highly complex with literally hundreds of different possible proteins arising due to extensive alternative splicing at both the 5' and 3' ends, as well as alternative promoter usage. Much more work will be required to understand how aberrant methylation in CaP affects this complex system.

When we investigated whether some of the methylation events identified in the TRAMP model were conserved in the human disease, we found that the human ortholog to the mouse RLGS spot 2G63 (BC029292) was methylated in 42% of human RCaP with very little methylation in AS-BP and only slightly more in AS-CaP. The human *NRXN2* CpG island, however, was not methylated in any human samples. The NRXN2 gene product is involved in synaptic adhesion and is expressed in neurons. Interestingly, in the TRAMP mouse, where we observed a high frequency of methylation in PRIM and AIP tumors, a neuroendocrine phenotype is very commonly observed in late stage primary and androgen-independent tumors, but less commonly in metastatic tumors (9). However, in the human disease, where we did not observe *NRXN2* methylation, a primarily neuroendocrine phenotype is much less common (9, 53, 54). It is likely that the expression of *Nrxn2* in tumors with a high neuroendocrine component is reflective of the fact that a large proportion of the tumor cells have taken on a neuroendocrine phenotype, and may in fact prove to be an effective marker of the phenotype. These observations suggest that the TRAMP model may be a very useful tool for the identification of novel targets of aberrant CpG island hypermethylation in human CaP, but that there will also be differences; some of which are likely to be at genes whose function contributes to different characteristics between the mouse model and the human disease.

We have demonstrated that aberrant DNA methylation plays a significant role in the TRAMP mouse model. The finding of phenotype-specific methylation events, particularly those events unique to tumors found at the primary site, but not at the metastatic sites, suggests that epigenetics in general, and DNA methylation in particular, may play an important role in advanced CaP. To a lesser degree, we also demonstrated differences in methylation patterns between primary tumors and androgen-independent recurrences. These loci identified by genomic scanning in this mouse model can be used in a candidate gene approach to study the advanced phenotypes of the human disease in the very limited samples that are available and generally not amenable to genome wide screens.

Acknowledgements

The authors would like to acknowledge the excellent technical assistance of Angela Szafranek. This work was supported in part by the National Cancer Institute through the Roswell Park Cancer Center Support Grant, [CA 16056], NCI R21 CA121216 (MC and DJS), R21 CA128062 (ARK), NIH 5T32CA009072 (SMK), DOD PC060354 (SMK), and PO1-NCI-CA77739 (JLM).

References

1. Nelson WG, De Marzo AM, Isaacs WB. Prostate cancer. N Engl J Med 2003;349:366-81.
2. Byar DP. Proceedings: The Veterans Administration Cooperative Urological Research Group's studies of cancer of the prostate. Cancer 1973;32:1126-30.
3. Labrie F, Belanger A, Dupont A, Luu-The V, Simard J, Labrie C. Science behind total androgen blockade: from gene to combination therapy. Clin Invest Med 1993;16:475-92.
4. Baylin SB, Herman JG, Graff JR, Vertino PM, Issa JP. Alterations in DNA methylation: a fundamental aspect of neoplasia. Adv Cancer Res 1998;72:141-96.
5. Gama-Sosa MA, Wang RY, Kuo KC, Gehrke CW, Ehrlich M. The 5-methylcytosine content of highly repeated sequences in human DNA. Nucleic Acids Res 1983;11:3087-95.
6. Costello JF, Plass C. Methylation matters. J Med Genet 2001;38:285-303.
7. Jones PA. Cancer. Death and methylation. Nature 2001;409:141, 3-4.
8. Laird PW. The power and the promise of DNA methylation markers. Nat Rev Cancer 2003;3:253-66.
9. Salem CE, Markl ID, Bender CM, Gonzales FA, Jones PA, Liang G. PAX6 methylation and ectopic expression in human tumor cells. Int J Cancer 2000;87:179-85.
10. Nguyen C, Liang G, Nguyen TT, Tsao-Wei D, Groshen S, Lubbert M, et al. Susceptibility of nonpromoter CpG islands to de novo methylation in normal and neoplastic cells. J Natl Cancer Inst 2001;93:1465-72.
11. Morey SR, Smiraglia DJ, James SR, Yu J, Moser MT, Foster BA, et al. DNA methylation pathway alterations in an autochthonous murine model of prostate cancer. Cancer Res 2006;66:11659-67.
12. Smith JF, Mahmood S, Song F, Morrow A, Smiraglia D, Zhang X, et al. Identification of DNA Methylation in 3' Genomic Regions that are Associated with Upregulation of Gene Expression in Colorectal Cancer. Epigenetics 2007;2.
13. Verma M, Srivastava S. Epigenetics in cancer: implications for early detection and prevention. Lancet Oncol 2002;3:755-63.
14. Smiraglia DJ, Plass C. The development of CpG island methylation biomarkers using restriction landmark genomic scanning. Ann N Y Acad Sci 2003;983:110-9.
15. Harden SV, Guo Z, Epstein JI, Sidransky D. Quantitative GSTP1 methylation clearly distinguishes benign prostatic tissue and limited prostate adenocarcinoma. J Urol 2003;169:1138-42.
16. Jeronimo C, Usadel H, Henrique R, Oliveira J, Lopes C, Nelson WG, et al. Quantitation of GSTP1 methylation in non-neoplastic prostatic tissue and organ-confined prostate adenocarcinoma. J Natl Cancer Inst 2001;93:1747-52.
17. Lodygin D, Epanchintsev A, Menssen A, Diebold J, Hermeking H. Functional Epigenomics Identifies Genes Frequently Silenced in Prostate Cancer. Cancer Res 2005;65:4218-27.
18. Wu M, Ho SM. PMP24, a gene identified by MSRF, undergoes DNA hypermethylation-associated gene silencing during cancer progression in an LNCaP model. Oncogene 2004;23:250-9.

19. Smiraglia DJ, Rush LJ, Fruhwald MC, Dai Z, Held WA, Costello JF, et al. Excessive CpG island hypermethylation in cancer cell lines versus primary human malignancies. Hum Mol Genet 2001;10:1413-9.
20. Greenberg NM, DeMayo F, Finegold MJ, Medina D, Tilley WD, Aspinall JO, et al. Prostate cancer in a transgenic mouse. Proc Natl Acad Sci U S A 1995;92:3439-43.
21. Gingrich JR, Barrios RJ, Morton RA, Boyce BF, DeMayo FJ, Finegold MJ, et al. Metastatic prostate cancer in a transgenic mouse. Cancer Res 1996;56:4096-102.
22. Eng MH, Charles LG, Ross BD, Chrisp CE, Pienta KJ, Greenberg NM, et al. Early castration reduces prostatic carcinogenesis in transgenic mice. Urology 1999;54:1112-9.
23. Gingrich JR, Barrios RJ, Kattan MW, Nahm HS, Finegold MJ, Greenberg NM. Androgen-independent prostate cancer progression in the TRAMP model. Cancer Res 1997;57:4687-91.
24. Mohler JL, Gregory CW, Ford OH, 3rd, Kim D, Weaver CM, Petrusz P, et al. The androgen axis in recurrent prostate cancer. Clin Cancer Res 2004;10:440-8.
25. Berthon P, Dimitrov T, Stower M, Cussenot O, Maitland NJ. A microdissection approach to detect molecular markers during progression of prostate cancer. Br J Cancer 1995;72:946-51.
26. Smiraglia DJ, Frühwald MC, Costello JF, McCormick SP, Dai Z, Peltomäki P, et al. A New Tool for the Rapid Cloning of Amplified and Hypermethylated Human DNA Sequences from Restriction Landmark Genome Scanning Gels. Genomics 1999;58:254-62.
27. Dai Z, Zhu WG, Morrison CD, Brena RM, Smiraglia DJ, Raval A, et al. A comprehensive search for DNA amplification in lung cancer identifies inhibitors of apoptosis cIAP1 and cIAP2 as candidate oncogenes. Hum Mol Genet 2003;12:791-801.
28. Yu L, Liu C, Bennett K, Wu YZ, Dai Z, Vandeusen J, et al. A NotI-EcoRV promoter library for studies of genetic and epigenetic alterations in mouse models of human malignancies. Genomics 2004;84:647-60.
29. Zardo G, Tiirikainen MI, Hong C, Misra A, Feuerstein BG, Volik S, et al. Integrated genomic and epigenomic analyses pinpoint biallelic gene inactivation in tumors. Nat Genet 2002;32:453-8.
30. Smiraglia DJ, Kazhiyur-Mannar R, Oakes CC, Wu YZ, Liang P, Ansari T, et al. Restriction Landmark Genomic Scanning (RLGS) spot identification by second generation virtual RLGS in multiple genomes with multiple enzyme combinations. BMC Genomics 2007;8:446.
31. Ehrich M, Nelson MR, Stanssens P, Zabeau M, Liloglou T, Xinarianos G, et al. Quantitative high-throughput analysis of DNA methylation patterns by base-specific cleavage and mass spectrometry. Proc Natl Acad Sci U S A 2005;102:15785-90.
32. Coolen MW, Statham AL, Gardiner-Garden M, Clark SJ. Genomic profiling of CpG methylation and allelic specificity using quantitative high-throughput mass spectrometry: critical evaluation and improvements. Nucleic Acids Res 2007;35:e119.

33. Costello JF, Fruhwald MC, Smiraglia DJ, Rush LJ, Robertson GP, Gao X, et al. Aberrant CpG-island methylation has non-random and tumour-type-specific patterns. Nat Genet 2000;24:132-8.
34. Smiraglia DJ, Plass C. The study of aberrant methylation in cancer via restriction landmark genomic scanning. Oncogene 2002;21:5414-26.
35. Shen L, Guo Y, Chen X, Ahmed S, Issa JP. Optimizing annealing temperature overcomes bias in bisulfite PCR methylation analysis. Biotechniques 2007;42:48, 50, 2 passim.
36. Warnecke PM, Stirzaker C, Melki JR, Millar DS, Paul CL, Clark SJ. Detection and measurement of PCR bias in quantitative methylation analysis of bisulphite-treated DNA. Nucleic Acids Res 1997;25:4422-6.
37. Missler M, Zhang W, Rohlmann A, Kattenstroth G, Hammer RE, Gottmann K, et al. Alpha-neurexins couple Ca2+ channels to synaptic vesicle exocytosis. Nature 2003;423:939-48.
38. Ushkaryov YA, Sudhof TC. Neurexin III alpha: extensive alternative splicing generates membrane-bound and soluble forms. Proc Natl Acad Sci U S A 1993;90:6410-4.
39. Ushkaryov YA, Petrenko AG, Geppert M, Sudhof TC. Neurexins: synaptic cell surface proteins related to the alpha-latrotoxin receptor and laminin. Science 1992;257:50-6.
40. Tabuchi K, Sudhof TC. Structure and evolution of neurexin genes: insight into the mechanism of alternative splicing. Genomics 2002;79:849-59.
41. Smiraglia DJ, Smith LT, Lang JC, Rush LJ, Dai Z, Schuller DE, et al. Differential targets of CpG island hypermethylation in primary and metastatic head and neck squamous cell carcinoma (HNSCC). J Med Genet 2003;40:25-33.
42. Smith LT, Lin M, Brena RM, Lang JC, Schuller DE, Otterson GA, et al. Epigenetic regulation of the tumor suppressor gene TCF21 on 6q23-q24 in lung and head and neck cancer. Proc Natl Acad Sci U S A 2006;103:982-7.
43. Hartwell KA, Muir B, Reinhardt F, Carpenter AE, Sgroi DC, Weinberg RA. The Spemann organizer gene, Goosecoid, promotes tumor metastasis. Proc Natl Acad Sci U S A 2006;103:18969-74.
44. Kaplan-Lefko PJ, Chen TM, Ittmann MM, Barrios RJ, Ayala GE, Huss WJ, et al. Pathobiology of autochthonous prostate cancer in a pre-clinical transgenic mouse model. Prostate 2003;55:219-37.
45. Bonkhoff H. Neuroendocrine differentiation in human prostate cancer. Morphogenesis, proliferation and androgen receptor status. Ann Oncol 2001;12 Suppl 2:S141-4.
46. Nelson EC, Cambio AJ, Yang JC, Ok JH, Lara PN, Jr., Evans CP. Clinical implications of neuroendocrine differentiation in prostate cancer. Prostate Cancer Prostatic Dis 2007;10:6-14.

Figure legends

Figure 1) Global analysis of RLGS data. A) Plot showing the number of RLGS spots lost in each of the 30 tumor sample RLGS profiles in each of the three phenotypes: primary, androgen-independent primary, and metastatic tumors. The dotted lines represent the median number of spots lost in each group, and the bars represent the interquartile range. B) Frequency distribution for RLGS spot loss showing the percentage of spots lost in the number of tumors indicated on the X axis. The percentages are taken from the total number of spots lost at least once in each of the three phenotypes (222, 212, and 270 spots each for primary, androgen-independent primary, and metastatic tumors, respectively). C) Venn diagram of RLGS spot loss comparing the specific loci methylated in the three tumor phenotypes and limited to those spots lost three or more times within a phenotype.

Figure 2) Mass Array Quantitative Methylation Analysis (MAQMA) of three RLGS loci on the entire sample set. A-C) The average level of methylation detected by MAQMA across the sequenced fragment of the CpG islands for each samples is shown on the Y axis. This value comes from taking the average of MAQMA values for each CpG dinucleotide sequenced for each sample. The samples are divided up categorically by phenotype (PRIM, MET, or AIP) and the RLGS status (methylated or unmethylated) for each spot along the X axis. Each symbol represents a single sample. D) To test for bisulfite PCR bias we used peripheral blood lymphocyte (PBL) DNA as a 0% methylation control, and an *in vitro* methylated (IVM) aliquot of the same DNA as a 100% methylated control. These DNAs were mixed at appropriate ratios to generate 75%, 50%, and 25% methylated controls and all the controls were bisulfite treated and used as template for bisulfite PCR and MAQMA analysis. The data are presented in a XY scatter plot with the observed methylation values (average MAQMA values as in A-C) on the Y axis plotted against the expected methylation values based on the ratios of PBL DNA to IVM PBL DNA used as template. The results of a theoretically perfect experiment are shown as a straight line with closed circles. All data points below this line represent PCR bias against the methylated alleles.

Figure 3) Genomic structure, DNA methylation, and expression of genes. A) Cartoon of the genomic structure of the BC058385 mRNA 57kb locus, and of the of the Gsc 2kb locus. The CpG island and the NotI site represented by the RLGS spot 2G63 are shown and fall in exon 4. The CpG island and the NotI site represented by the RLGS spot 3C21 are shown. The MAQMA and qRT-PCR primers are shown. B) SYBR green qRT-PCR results plotted against MAQMA results in an XY scatter plot. SYBR green qRT-PCR was performed on 15 samples from each of the three phenotypes and normal prostate cDNA and normalized to 18s rRNA levels. C) SYBR green qRT-PCR results for *Gsc* plotted against RLGS status. SYBR green qRT-PCR was performed on 10 samples from each of the three phenotypes and normalized to 18s rRNA levels. D) Same as in C) except plotted by phenotype and RLGS status.

Figure 4) Genomic structure, DNA methylation, and expression of the *Nrxn2* locus. Cartoon of the genomic structure of the Nrxn2 105kb locus. A) SYBR green qRT-PCR results for *Nrxn2*α plotted against RLGS status. B) Same as in A) except plotted against

phenotype. C) SYBR green qRT-PCR results for *Nrxn2β* plotted against RLGS status. D) Same as in C) except plotted against phenotype.

Figure 5) MAQMA data for the human ortholog to mouse 2G63 CpG island on human prostate tissues. Each line represents a single sample, with each circle representing a CpG dinucleotide. The percent methylation at each CpG is indicated by the grey scale shading of each circle according to the key at the top of the figure. CpG dinucleotides for which no data could be obtained are shown as a grey, dashed circle. The number to the left of each line indicates the sample number. A) Data for 13 androgen-stimulated benign prostate (AS-BP), B) Data for 13 androgen-stimulated primary prostate cancer (AS-CaP), C) Data for 12 primary tumor recurrences after androgen deprivation therapy (RCaP), D) The average level of methylation detected by MAQMA across the sequenced fragment of the CpG islands for each samples is shown on the Y axis. This value comes from taking the average of MAQMA values for each CpG dinucleotide sequenced for each sample. The samples are divided up categorically by phenotype (AS-BP, AS-CaP, or RCaP) along the X axis. Each symbol represents a single sample.

Table 1 RLGS spots of interest.

#	Spot	PRIM n=30	MET n=30	AIP n=30	Total n=90	Class	[d]P-value	[e]CGI	Context	[h]Gene Homology
1	3C21	**20**	1	**27**	48	[a]Prim or AIP	**1.0E-12**	Y	Body	**Nrxn2**
2	3E30	**24**	5	**29**	58	Prim or AIP	**2.3E-11**	N	3'end	**Gsc**
3	5F09	**19**	2	**21**	42	Prim or AIP	**2.5E-08**	N	Body	**Cacna1a**
4	2G63	**22**	8	**29**	59	Prim or AIP	**7.1E-08**	Y	Body	**BC058385**
5	2B37	**14**	1	**14**	29	Prim or AIP	**1.0E-05**	[f]--	--	--
6	5B30	**20**	6	**22**	48	Prim or AIP	**1.2E-05**	Y	Body	**AK139829**
7	4D27	**16**	6	**19**	41	Prim or AIP	**7.0E-04**	Y	[g]5'end	**Hoxa2**
8	3E16	**8**	0	**8**	16	Prim or AIP	**9.1E-04**	--	--	--
9	4C01	**18**	9	**20**	47	Prim or AIP	**3.0E-03**	Y	5'end	**AK044818**
10	3D01	**7**	0	**7**	14	Prim or AIP	**3.0E-03**	--	--	--
11	2G10	**8**	0	**6**	14	Prim or AIP	**3.8E-03**	--	--	--
12	2C17	**7**	0	**5**	12	Prim or AIP	**7.0E-03**	--	--	--
13	4C17	**13**	8	**20**	41	Prim or AIP	**1.4E-02**	Y	5' end	**Lhfpl4**
14	4D69	0	0	**9**	9	[b]AIP specificity	**2.0E-05**	Y	5'end	**Nfyb**
15	4E04	2	4	**15**	21	AIP specificity	**5.0E-05**	Y	5'end	**Tpm2**
16	4D54	0	5	**14**	19	AIP specificity	**6.0E-05**	Y	5'end	**Pawr**
17	4E16	0	1	**9**	10	AIP specificity	**1.0E-04**	Y	5'end	**Tpm2**
18	3C39	0	0	**7**	7	AIP specificity	**2.0E-04**	Y	5'end	**Mid1ip1**
19	3G88	5	2	**13**	20	AIP specificity	**1.0E-03**	Y	5'end	**Il6st**
20	3D22	29	23	30	**82**	[c]Frequency		N	3'end	**Cdkn2a**
21	4C11	21	25	28	**74**	Frequency		N	Body	**4932416N17Rik**
22	4E25	23	25	26	**74**	Frequency		--	--	--
23	4C38	19	15	28	**62**	Frequency		Y	5' end	**Lhfpl4**
24	4C31	23	11	25	**59**	Frequency		N	Body	**Adcy5**
25	4C13	23	9	26	**58**	Frequency		Y	5'end	**AK039621**
26	3D67	18	17	21	**56**	Frequency		Y	3'end	**Oprd1**
27	2C28	16	14	22	**52**	Frequency		Y	5'end	**AK004006**
28	2E04	19	9	13	**41**	Frequency		--	--	--
29	2D21	13	8	15	**36**	Frequency		Y	3'end	**BC025575**
30	3E56	9	11	15	**35**	Frequency		Y	5' end	**Zfp787**
31	3E07	7	12	16	**35**	Frequency		Y	5'end	**U2af1-rs1**
32	6D10	6	12	15	**33**	Frequency		N	Intergenic	**Intergenic**

[a]Spots lost significantly in primary tumors plus androgen-independent primary tumors (n=60), but not metastatic tumors (n=30); [b]Spots lost significantly in androgen-independent primary tumors (n=30), but not in primary plus metastatic tumors (n=60); [c]Spots lost in greater than 30 samples from all tumor types (n=90); [d]Fischer's Exact test (two-tailed) for class membership; [e]Is the RLGS spot NotI site within 200bp of a CpG island; [f]RLGS spot is unidentified; [g]Within 5kb of transcriptional start site and/or including exon 1; [h]Annotated gene, mRNA, or spliced EST within 5 kb of the CpG island or NotI site.

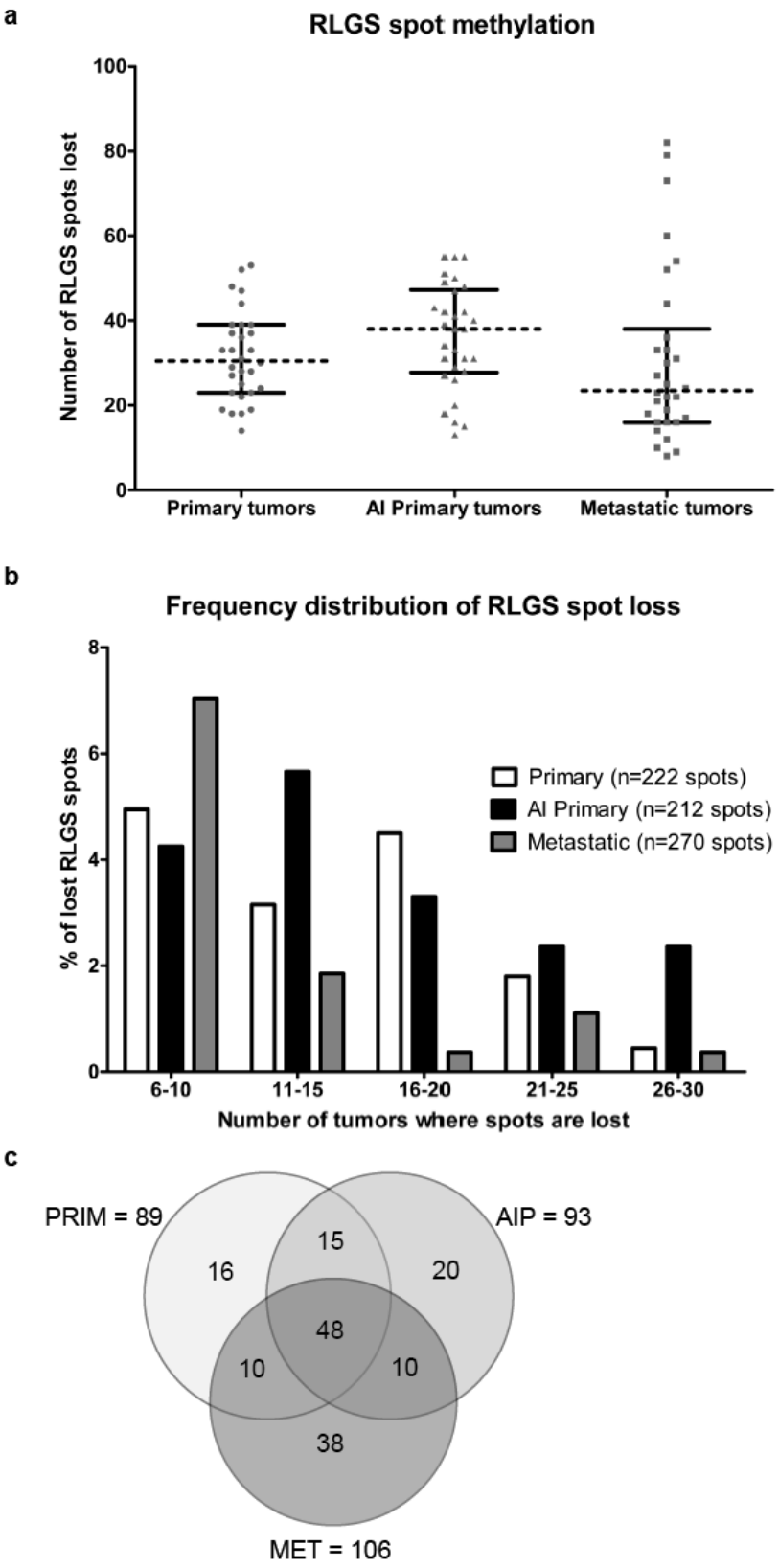

Figure 1. Camoriano et al.

Figure 2 Camoriano et al.

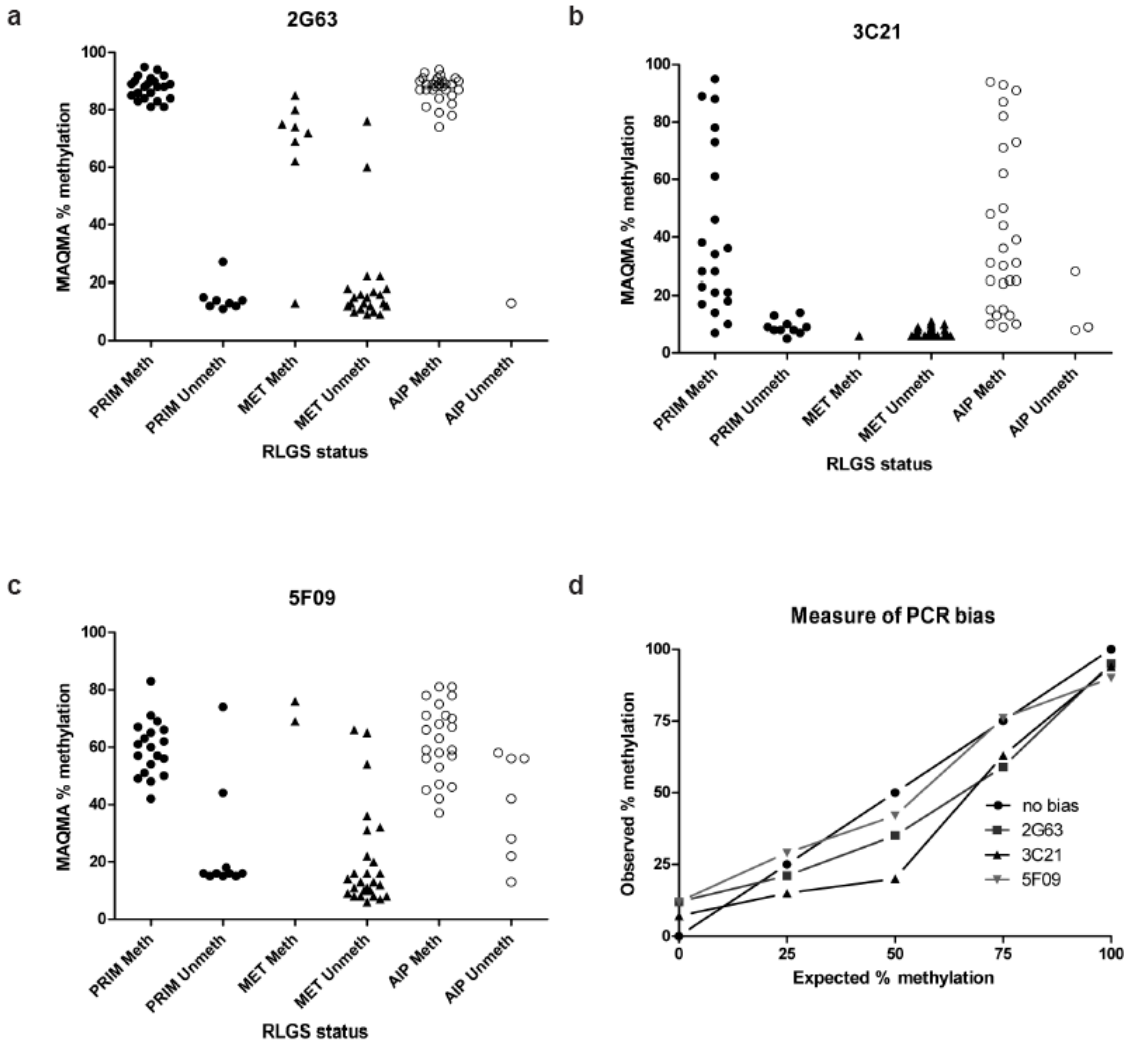

Figure 3 Camoriano et al.

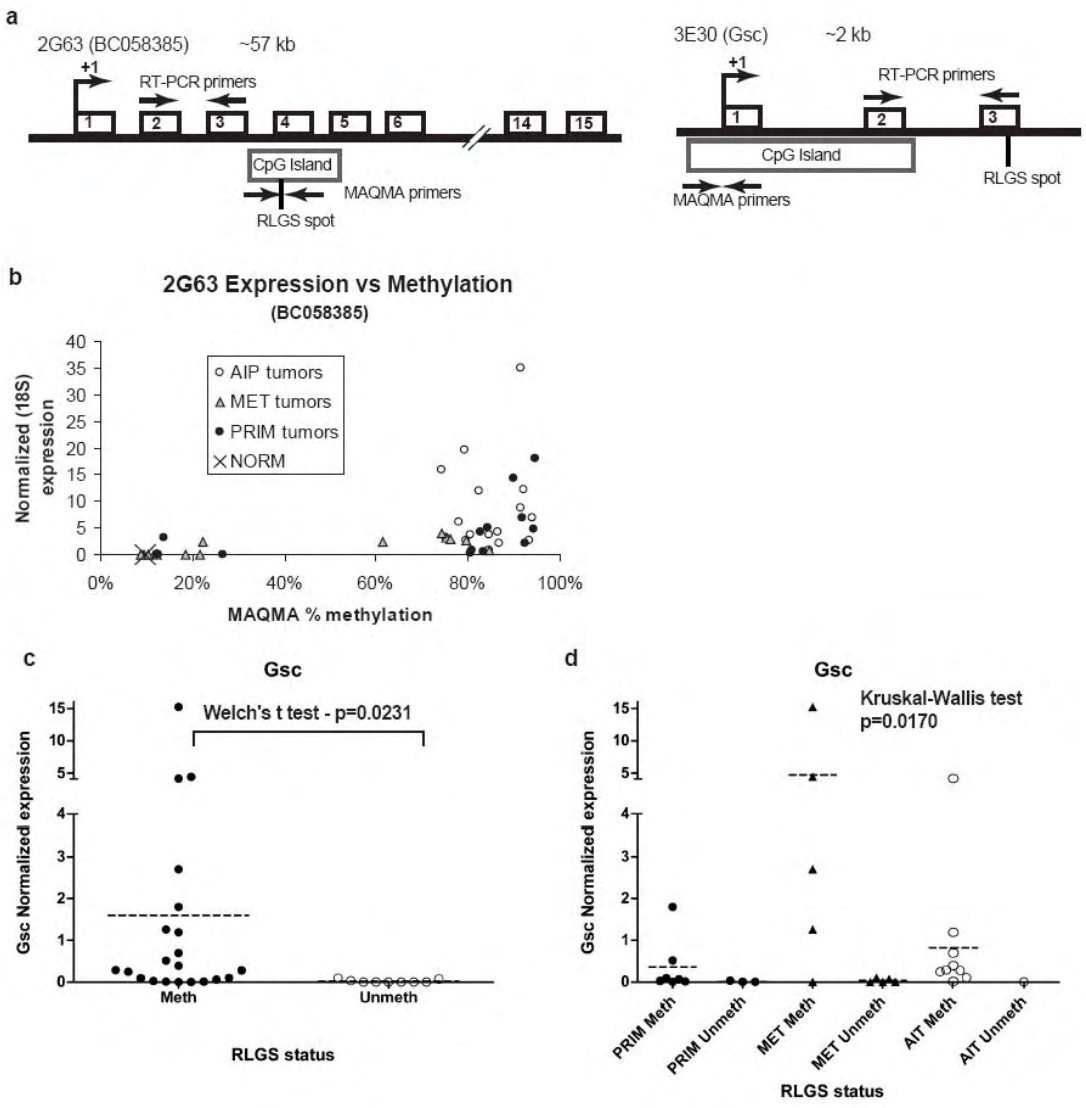

Figure 4 Camoriano et al.

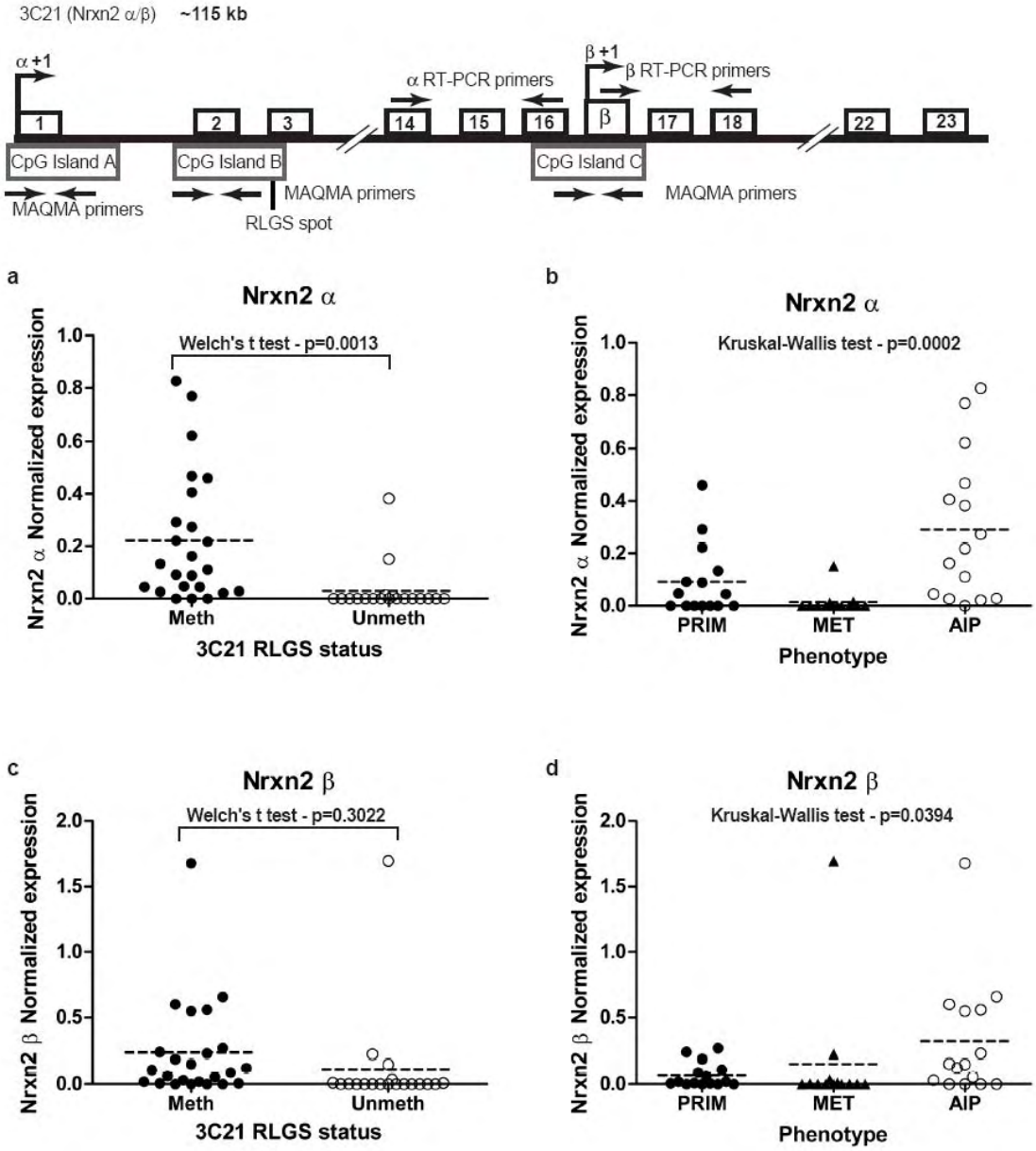

Figure 5. Camoriano et al.